DEVELOPMENT OF INTENSITY-DURATION-FREQUENCY CURVES USING LOCAL AND REGIONAL SCALE METHODS

DEVELOPMENT OF INTENSITY-DURATION-FREQUENCY CURVES USING LOCAL AND REGIONAL SCALE METHODS

By: Marc D'Alessandro, B.Sc

A Thesis Submitted to the School of Graduate Studies in Partial Fulfillment of the Requirement for the Degree of Master of Science

MASTER OF SCIENCE (2016) McMaster University

(Geography and Earth Science) Hamilton, Ontario

TITLE: Development of Intensity-Duration-Frequency Curves Using Local and Regional Scale Methods

AUTHOR: Marc D'Alessandro, B.Sc (McMaster University)

SUPERVISOR: Dr. Paulin Coulibaly

NUMBER OF PAGES: xv, 84

Abstract

Traditionally civil infrastructure designs were rendered using rainfall data from dated historical records. However, recent studies have shown that the magnitude and intensity of historical precipitation events do not exhibit the extreme nature of precipitation events that are projected to occur in the future. Increasing extreme rainfall trends have already been documented in Canada. Therefore there are growing concerns that the aging infrastructure in southern Ontario will be unable to function effectively and as a result the frequency of floods is expected to increase. Updating intensity-duration-frequency (IDF) curves to account for extreme precipitation events is vital to ensure that the consequences of floods are mitigated. This study first reviewed the most robust techniques for updating IDF curves, and applied a select set of approaches to create IDF curves for stations within southern Ontario.

Three robust techniques – the at-site method, the regional frequency analysis method, and a future IDF curve development technique – were compared with one another to determine which technique was most suitable for updating IDF curves in southern Ontario. Results showed that the difference between the at-site method and the regional frequency analysis method was marginal for short return periods, however for larger return periods larger differences were observed. Future IDF statistic results showed that for the 2050s there were minor differences in the increases in rainfall intensities when comparing with the at-site and the regional frequency analysis method. For the 2100s there were larger increases in rainfall intensities compared to the at-site and the regional frequency analysis method, especially for larger return periods. These results suggest that it is worthwhile for regions within southern Ontario to update their IDF curves using the future IDF curve technique, however it is recommended that additional climate

models, emission scenarios and downscaling techniques involved in future IDF curve construction are explored.

Acknowledgements

I would like to thank my supervisor, Dr. Coulibaly, for all of his guidance and support throughout my graduate studies. Dr. Coulibaly's encouragement enabled me to reach all of my goals and for that I am very appreciative. I would also like to thank my mom and dad, my sister, my grandparents and all of my family and friends for their support. I would also like to thank Serge Traore, Dr. Tara Razavi, Dr. Niko Yiannakoulias, Dr. Hussein Wazneh and everybody from McMaster's Hydrologic Modeling and Water Resources Lab for all of their help and guidance.

Table of Contents

List of Figures

List of Tables

List of Abbreviations

AMS	Annual Maximum Series
CanRCM4-CanESM2	The fourth generation of the Canadian regional climate model driven by the second generation of the Canadian earth system model.
GCM	Global Climate Model
GEV	Generalized Extreme Value
GHG	Greenhouse gas
GLO	Generalized Logistic
GNO	Generalized Normal
GPD	Generalized Pareto
HadGEM2-ES	The Hadley Global Environment Model 2 coupled with the earth system model.
IDF	Intensity-duration-frequency
IPCC	Intergovernmental Panel on Climate Change
PCs	Principal Components
PCA	Principal Component Analysis
PDS	Partial duration series
PE3	Pearson Type III
RCP	Representative Concentration Pathways
RCM	Regional Climate Model
RFA	Regional Frequency Analysis

List of Symbols

a	Coefficient which is equal to 0
b	Linear regression coefficient
c	The 24-hour precipitation value
C	The total cost function for the entire regionalization plan
d	The ratio value used to obtain the desired hourly or sub-hourly data value
Px_1	The station with a missing precipitation value
Px_2	The nearest neighbouring station's respective precipitation value
X	The converted precipitation value for a desired duration
V_{x1}	The total within-region variation in mean annual precipitation for all sites
V_{x2}	The total within-region variation in spring precipitation for all sites
V_{x3}	The total within-region variation in summer precipitation for all sites
V_{x4}	The total within-region variation in fall precipitation for all sites
V_{x5}	The total within-region variation in winter precipitation for all sites
V_{x6}	The total within-region variation in 100 maximum daily precipitation values for all sites
V_{x7}	The non-connectivity penalty
Z^{DIST}	Goodness-of-fit measure
τ_3	L-moment coefficient of skewness
τ_4	L-moment coefficient of kurtosis

1. Introduction

1.1 Background and Rationale

Intensity-duration-frequency (IDF) curves are utilized by water resources engineers to design hydraulic structures such as sewer systems, dams and culverts. Previously IDF curves were developed using historical rainfall data however recent observations and studies indicate that historical data does not represent the intensity and magnitude of rainfall events that are expected to occur in the future. Climate change impact studies from across North America have predicted increasing trends in extreme rainfall events and such information needs to be accounted for in design storm estimation. Infrastructure failure is a major concern because it can lead to flooding which has proven to negatively impact society. There were recent cases in southern Ontario where extreme rainfall events led to severe flooding. On July 8, 2013 an intense storm in Toronto, Ontario caused approximately $1 billion in damages due to homes being flooded, power outages and roads being flooded (Environment and Climate Change Canada, 2015). Furthermore, on August 4, 2014 a large storm in Burlington, Ontario caused $90 million in damages due to homes and commercial buildings being flooded, damage to driveway culverts and the flooding of car parking areas (Conservation Halton, 2015). Therefore updating IDF curves to account for extreme rainfall events is required to ensure that the aforementioned consequences of floods are prevented.

Climate change is caused by anthropogenic greenhouse gas emissions being produced at an excessive rate. Approximately 50% of anthropogenic carbon dioxide emissions have occurred within the last 40 years (IPCC, 2014). Greenhouse gas emissions are expected to increase in the future and climate scientists believe that there will be unduly consequences on the Earth's

climate, including increases in the magnitude and intensity of extreme rainfall events. Accounting for these projected increases is extremely important for infrastructure design, therefore the use of future climate models is necessary when designing water system infrastructure (Lemmen, 2008). Different scenarios project greenhouse gas emission rates for the entire 21st century based on global population, energy use and land use practices and resulting precipitation intensity responses can be computed using climate models (IPCC, 2014). Regional climate models and global climate models are used in this study to determine future precipitation intensities triggered by climate change for the southern Ontario region.

1.2 Study Objectives

This research is part of the NSERC Canadian FloodNet Research Program, specifically Project 1-4: Development of new methods for updating IDF curves in Canada.

The specific objective of this study was to update IDF curves in southern Ontario using emerging methodologies. This study assessed several methodologies for updating IDF curves and a comparative analysis was completed to determine which technique is most suitable for updating IDF curves in southern Ontario. The objectives of this study are summarized as follows:

1. Identify weather stations located within southern Ontario that meet the requirements of this study and collect daily precipitation data for each station.
2. Identify the most effective IDF curve methodologies and update the IDF curves for each station located within the study area using these methodologies;

a. Apply the *at-site method* to update IDF curves, specifically fitting the generalized extreme value (GEV) probability distribution function to the annual maximum rainfall data for each station.
b. Apply the *regional frequency analysis method* to update IDF curves. Utilize clustering techniques such as Principal Component Analysis (PCA) with k-means, Ward's method and Tabreg to classify weather stations into homogeneous precipitation regions. Apply the L-moments approach to determine if the delineated regions were statistically homogeneous and for quantile estimation.
c. Apply the *future IDF curve method* to update IDF statistics. Use the Delta change method for statistical downscaling and use a combination of two climate model outputs (CanRCM4-CanESM2 and HadGEM2-ES) and two emission scenarios (RCP4.5 and RCP8.5) to establish future rainfall intensities.

3. Perform a comparative analysis for the three aforementioned techniques and identify the technique that is most suitable for updating IDF curves in southern Ontario.

1.3 Organization of Thesis

Chapter 2 contains a literature review which outlines the development of IDF curve techniques over time. Chapter 3 presents the study area and a description of the data that was used. Chapter 4 outlines the methodologies utilized throughout this study. Chapter 5 presents and discusses the results of the study. Chapter 6 provides the conclusions of the study, and Chapter 7 outlines recommendations for future work.

2. Literature Review

2.1 The At-Site Intensity-Duration-Frequency (IDF) Curve Method

The at-site method which is used for IDF curve derivation can be dated back to 1932 (Bernard, 1932). The at-site method uses frequency analysis to determine the recurrence of extreme rainfall events for a single site (or station). Various organizations have used the at-site method to update IDF curves for different regions throughout Canada. Coulibaly and Shi (2005) used the at-site method to develop updated IDF curves for the Grand River region and the Kenora and Rainy River region. The City of Guelph (2007) developed IDF curves for three weather stations using the at-site method and compared their results with the previously outdated IDF curves used for storm design. Shephard (2011) updated IDF curves using additional weather station data for New Brunswick, Nova Scotia, Newfoundland and Prince Edward Island with the at-site method. Paixao et al. (2011) utilized the at-site method to update IDF curves for 92 climate stations and 29 tipping bucket rain gauge stations in southern Ontario. Although the at-site method was once the conventional technique used for IDF curve derivation, there are limitations associated with this method. Skewed data obtained from weather stations could misrepresent the extreme nature of precipitation events due to short data records, a low density of weather stations in a large region and missing rainfall data. To circumvent this issue the regional frequency analysis method has become increasingly utilized for IDF curve development to overcome the limitations associated with the at-site method.

2.2 The Regional Frequency Analysis Method

The regional frequency analysis method (Hosking and Wallis, 1997) incorporates additional weather station data to enhance the characterization of extreme rainfall events for different regions. The regional frequency analysis method reduces uncertainties associated with

the at-site method by creating homogeneous regions which allows for additional rainfall data to be included in the derivation of IDF curves. The regional frequency analysis method has been used in studies to determine extreme rainfall rates and flood estimates for various study areas (Jingyi and Hall, 2004; Trefry et al., 2005; Schaefer et al., 2006; Parida and Moalafhi, 2008; Lim and Voeller, 2009; Saf, 2009; Ngongondo et al., 2011; Malekinezhad and Zare-Garizi, 2014; Bharath and Srinivas, 2015). A key component of the regional frequency analysis approach is the regionalization technique needed to define homogeneous regions.

2.2.1 Regionalization Techniques

One particularly important step in regional frequency analysis is the delineation of homogeneous regions using a clustering or classification technique. Hosking and Wallis (1997) recommend using Ward's method because it forms clusters containing an equal number of sites. Different studies have used a wide variety of clustering techniques to create homogeneous regions (Stathis and Myronidis, 2009; Abolverdi and Khalili, 2010; Modarres and Sarhadi, 2011; Paixao et al., 2011). The accuracy of the delineated regions is tested using the L-moment approach. Regions that are heterogeneous or contain discordant stations must be reevaluated to ensure that the inclusion of all sites within a cluster accurately represent similar hydrologic characteristics. Three clustering techniques, Principal Component Analysis with k-means clustering, Ward's method and Tabreg, were utilized to delineate regions exhibiting similar hydrologic characteristics for this study.

2.2.2 Principal Component Analysis and K-means Clustering

Principal Component Analysis (PCA) and k-means clustering have been utilized to delineate homogeneous regions when using the regional frequency analysis method. For

example, Brunnetti et al. (2004) applied PCA with VARIMAX rotation to monthly precipitation data for 39 stations located in Italy and analyzed long term precipitation trends for the 5 delineated regions. Maraun et al. (2008) analyzed seasonal precipitation trends in the United Kingdom by applying PCA to 689 rain gauge records that were categorized into 10 precipitation intensity classes. Stathis and Myronidis (2009) delineated homogeneous precipitation regions in central Greece by applying PCA to mean monthly precipitation data for 75 meteorological stations. Abolverdi and Khalili (2010) applied k-means to annual maximum precipitation data and at-site information, including latitude, longitude and elevation, and estimated quantiles for different return periods for 4 homogeneous regions in Iran. Bernard et al. (2013) applied k-means clustering to maximum hourly precipitation data in France and compared its results with the partitioning around medoids algorithm. Fragoso and Tildes Gomes (2008) utilized PCA with k-means clustering to determine spatial distribution patterns of heavy precipitation days and identified specific atmospheric circulation patterns contributing to heavy rainfall patterns in Portugal. Razavi and Coulibaly (2013) applied PCA with k-means clustering to delineate homogeneous watershed clusters in Ontario.

2.2.3 Ward's Method

Ward's method is a widely used clustering technique to allocate sites into homogeneous regions (Hosking and Wallis, 1997). Smithers and Schulze (2001) applied Ward's method to precipitation statistics and at-site characteristics of 172 rainfall stations in South Africa and created design storms for 15 regions, where 10 of the regions were considered acceptably homogeneous and 5 of the regions were considered possibly heterogeneous. Unal et al. (2003) applied Ward's method to temperature and precipitation data for 113 climate stations in Turkey and delineated 7 clusters that exhibited distinct climate characteristics. Muñoz-Diaz and Rodrigo

(2004) applied Ward's method to delineate homogeneous regions in Spain using seasonal rainfall data and compared their results with the PCA method. Kansakar et al. (2004) applied Ward's method to precipitation data in Nepal and determined the effect physical characteristics have on the seasonality of precipitation events and the magnitude of precipitation events. Kyselý et al. (2006) determined that Ward's method yielded superior results compared to the average-linkage clustering method and as a result four homogeneous regions which exhibited similar extreme precipitation characteristics in Czech Republic were identified. Noto and La Loggia (2009) applied Ward's method to 52 stream gauging sites in Sicily and developed growth curves to estimate flooding events for each region. Modarres and Sarhadi (2011) utilized Ward's method to delineate 8 rainfall regions in Iran and then applied L-moment statistics to determine the homogeneity, discordancy and regional frequency distribution function for each region. Paixao et al. (2011) applied k-means, centroid and Ward's method to 24 hour rainfall data in southern Ontario and determined that Ward's method was the most suitable technique to delineate homogeneous regions that exhibit similar precipitation patterns.

2.2.4 Tabreg

Tabreg (Yiannakoulias et al. 2007; Yiannakoulias and Bland, 2016) is a general purpose regionalization tool that is used to cluster stations into regions that exhibit similar hydrologic characteristics. Tabreg uses a greedy search algorithm to minimize a user defined cost function. The cost function can be comprised of multiple criteria and it is used to minimize within-region variability (Yiannakoulias and Bland, 2016). Tabreg is used for regionalization of weather stations, however this algorithm can be applied to other areas of study such as creating political districts or creating health care regions (Yiannakoulias and Bland, 2016).

2.3 Future IDF Curve Development Method

The at-site method and the regional frequency analysis method use historical rainfall data to determine recurrence intervals of extreme rainfall events. However the incorporation of climate model data is now commonly utilized when updating IDF curves. Practitioners need to develop infrastructure accounting for larger return periods and climate model data is used to develop design storms to withstand future rainfall extremes with a 50 year and 100 year return period. Climate change impact studies use regional climate models and global climate models to assess the impact future precipitation rates will have on society. The future climate model based technique has been used globally to determine rainfall rates that are expected to occur in the future (Hennessy et al., 1997; Xuejie et al., 2001; Mailhot et al., 2007; Mladjic et al., 2011; Dominguez et al., 2012; Mailhot et al., 2012; Willems et al., 2012; Clavet-Gaumont et al., 2013). Coulibaly and Shi (2005) used the Canadian Global Circulation Model-2 to develop future IDF curves for various regions in Ontario. Olsson et al. (2009) used the RCA3 regional climate model coupled with A2 and B2 emission scenarios and determined that there will be significant increases in extreme precipitation during the summer and autumn seasons in Kalmar, Sweden. Urrutia and Vuille (2009) used a regional climate model following the A2 and B2 scenarios for the 2070 – 2100 period and determined that different regions in the tropical Andes will experience both increases and decreases in precipitation rates. Feng et al. (2011) used a global climate model to project future precipitation changes in China and determined that extreme precipitation events would significantly increase in southeast China. Coulibaly et al. (2015) used an ensemble of global climate models and regional climate models to update IDF curves for weather stations located in the Toronto and Essex regions.

3. Study Area and Data

3.1 Study Area

The study area that will be assessed in this study is southern Ontario, Canada. Southern Ontario is the most populated region in Canada and it is a region that is projected to see its population increase in the future. Infrastructure development and expansion is expected and there is a need for IDF curves to accurately account for the extreme rainfall events that can impact this region. Selected 48 weather stations located within different areas of southern Ontario were used in this study (Figure 1). Between 1970 and 2000 the weather station with the highest mean annual precipitation was Chatsworth which had 1149 mm, and the weather station with the lowest mean annual precipitation was Toronto Island Airport which had a recording of 795 mm. The weather stations with the lowest altitude are Belleville and Frenchman's Bay with 76 meters above sea level, meanwhile Proton weather station had the highest altitude with 480 meters above sea level.

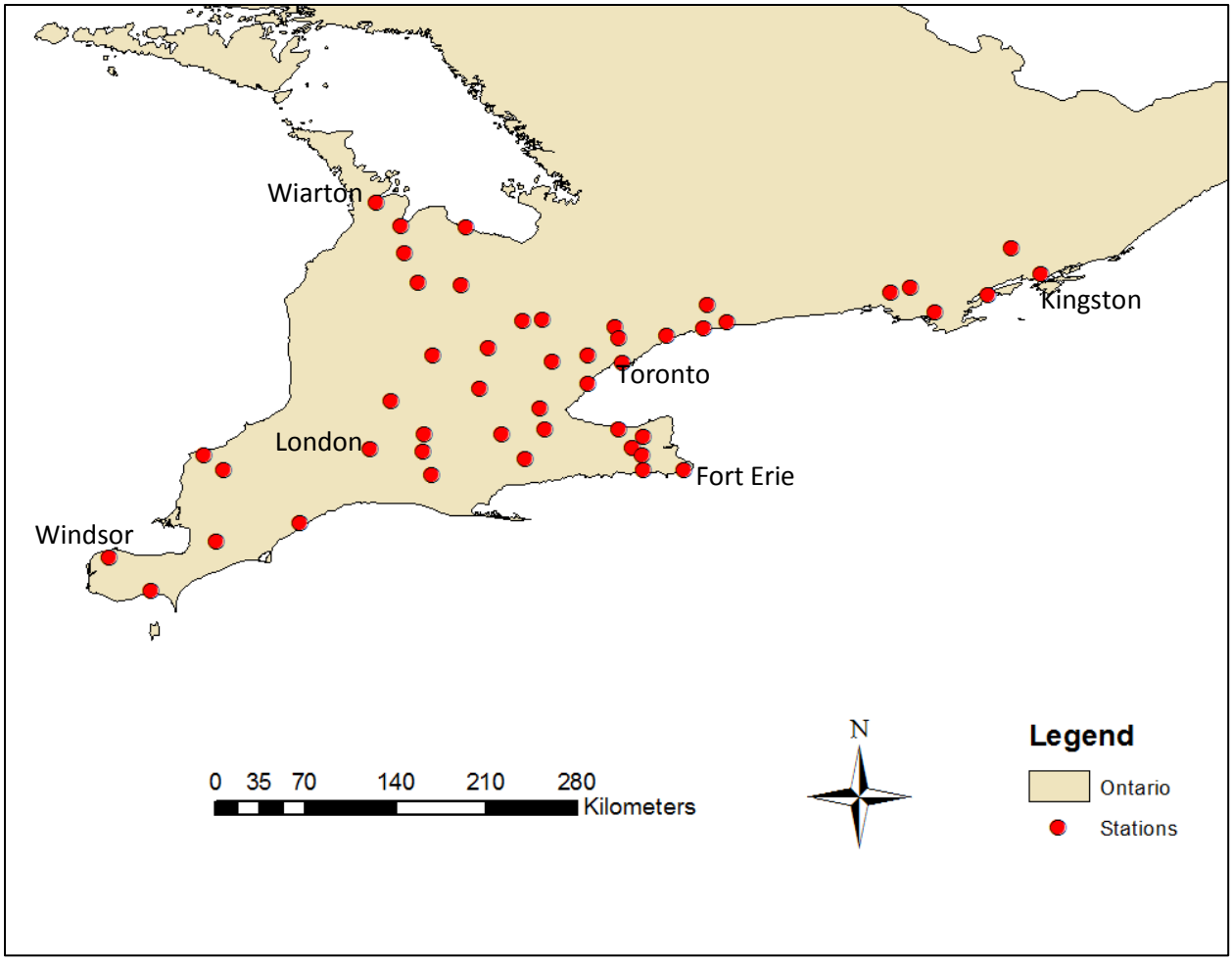

Figure 1: Map of southern Ontario showing the 48 weather stations used in the study.

3.2 Observed Data

31 years of daily precipitation data between 1970 and 2000 was collected from Environment Canada's Climate Data Archive for all 48 weather stations. A list of the selected weather stations is presented in Appendix A, also included in this list are geographic characteristics of each station such as latitude, longitude and altitude. There were specific criteria that each weather station had to fulfill before being selected for this study. The first criterion required each weather station to have at least 30 years of data. The second criterion was each station's most recent record of data must be recorded in the year 2000. The last criterion required

each station to have no more than 5% of its data missing. The weather station that had the most missing data was Cressy weather station and it had approximately 4% of its daily precipitation data missing.

Each weather station used in this study contained a large number of flagged data, i.e. estimated values and trace values. A table displaying the flagged data for each weather station can be found in Appendix B, Table B1. The weather station that contained the most trace values was Toronto Pearson Airport and approximately 20% of its daily precipitation data contained trace values. The weather station that contained the most estimated values was St. Catharines Power Glen and approximately 2% of its daily precipitation data contained estimated values. Although some weather stations contained a large number of flagged values this only affected the data used for the regionalization portion of the study. Environment Canada's weather station data exhibited substantial sources of error which is a limitation for the regionalization part of this study, however the annual maximum series data used to create the IDF curves was not estimated and considered more reliable.

3.3 Climate Model Data

Regional climate models (RCM) and global climate models (GCM) are commonly used for climate change impact studies in Ontario. The fourth generation of the Canadian regional climate model driven by the second generation of the Canadian Earth System Model (CanRCM4-CanESM2) was the RCM that was used in this study. The Hadley Global Environment Model 2 coupled with the Earth System Model (HadGEM2-ES) was the GCM that was used in this study. The CanRCM4-CanESM2 model data was downloaded from the Canadian Centre for Climate Modeling. The HadGEM2-ES model data was downloaded from

the PCMDI – Earth System Grid Federation. Details outlining characteristics such as spatial resolution, temporal resolution and simulation period for the CanRCM4-CanESM2 and HadGEM2-ES climate models can be found in Appendix C.

Climate model data for the current period (1970 - 2000) was collected for both climate models. Additionally, future climate model data was downloaded for the 2050s (2026 – 2045) and the 2100s (2081 – 2099) time periods for two emissions scenarios (RCP4.5 and RCP8.5) for both climate models. Determining future precipitation rates in response to climate change is achieved by looking at different scenarios which assess future global population, energy use and land use practices to project greenhouse gas emission rates for the 21st century (IPCC, 2014). These scenarios are known as Representative Concentration Pathways (RCPs). RCP4.5 is an intermediate scenario that limits the increase of future greenhouse gas emissions, meanwhile RCP8.5 is an intensive scenario which predicts that future greenhouse gas emissions will continually increase (IPCC, 2014).

4. Methodology

4.1 Overview of Methods

Initially weather stations were assessed to see if they would be suitable for this study. Additionally, an extensive review was conducted to determine the most robust techniques currently used for IDF curve development. After the review was conducted it was determined that the at-site method, the regional frequency analysis method and a future IDF curve method would be used to develop IDF curves for the selected weather stations. Figure 2 shows a flowchart of the methodology used for this study. Detailed description of each step of the methodology is provided hereafter.

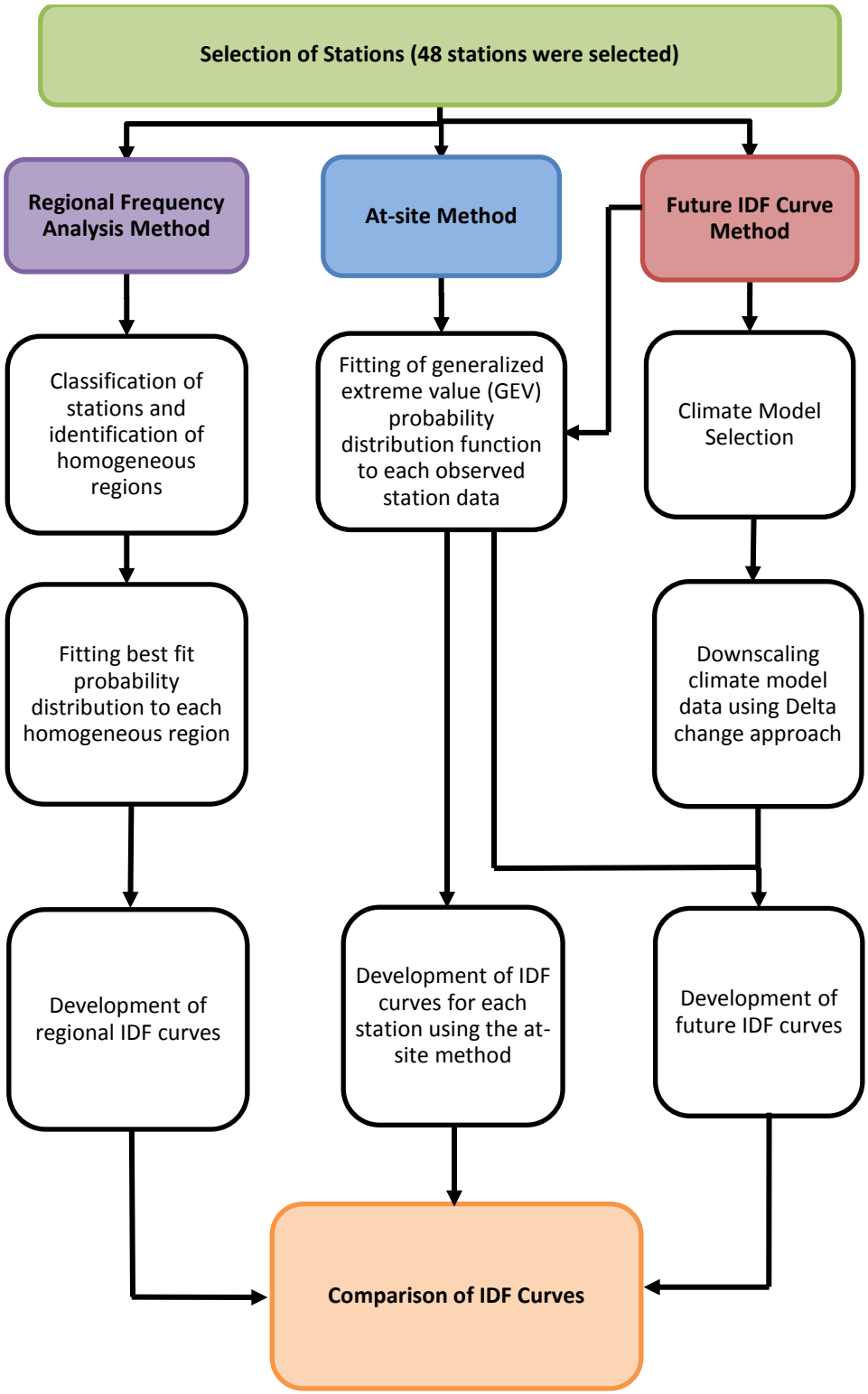

Figure 2: An overview of the methodology used in this study.

4.2 Data Processing

4.2.1 Converting Daily Duration Data to 24-hour Duration Data

The Environment Canada weather station data was provided in a daily duration format, however to create IDF curves for drainage design purposes the precipitation data must be in an hourly format. For all weather stations daily precipitation data was multiplied by 1.13, which is the Hershfield factor and it is commonly used to convert daily precipitation data to 24-hour duration data (Hershfield, 1961; Huff and Angel 1989; 1992; Coulibaly and Shi 2005; Coulibaly et al. 2015).

4.2.2 Replacing Flagged Data

Flagged data was replaced for each weather station using the following procedure, which is further described in Appendix B, Table B2:

1. All trace values were replaced with a value of 0.2 mm because this is the minimum recorded rainfall value from the dataset.
2. The “C” flag, which is defined as precipitation occurred but amount is uncertain, was replaced with a value of 0 mm.
3. The “A” flag, which is defined as accumulated precipitation where the previous value was the “C” flag, was replaced with a value of 0 mm.
4. The “E” flag, which is defined as an estimated value, already had a value in the dataset that was provided by Environment Canada, therefore the respective value remained intact.

5. The “F” flag, which is defined as an accumulated and estimated value, already had a value in the dataset that was provided by Environment Canada, therefore the respective value remained intact.
6. All missing data was replaced using a linear regression model between two nearest neighboring stations. The linear regression equation is formulated as,

$$Px_1 = a + bPx_2 \qquad (1)$$

where Px_1 is the station with a missing precipitation value, a is a coefficient which equals 0, b is the linear regression coefficient and Px_2 is the nearest neighbouring station’s respective precipitation value.

4.2.3 Converting 24-hour Duration Data to Hourly and Sub-Hourly Duration Data

Converting 24-hour precipitation data to hourly and sub-hourly data was completed using the ratio formula which was introduced by Hershfield (1961) and adapted by Huff and Angel (1989). The ratios were obtained from the Hydrological Atlas of Canada (1978) and can be viewed in Table 1. The ratio formula is defined as

$$X = c(d) \qquad (2)$$

where X is the converted precipitation value for a desired duration, c is the 24-hour precipitation value and d is the ratio value used to obtain the desired hourly or sub-hourly data value.

Rainfall Duration T_d (hours)	Ratio Converting 24-hour Data
18	0.91
12	0.82
6	0.73
3	0.64
2	0.56
1	0.45
0.50 (30 min.)	0.38
0.25 (15 min.)	0.29
0.17 (10 min.)	0.22
0.08 (5 min.)	0.12

Table 1: Coefficients of the Ratio formula for converting 24h rainfall to different hourly and sub-hourly durations of rainfall for Ontario (Adapted after Hershfield (1961); Huff and Angel (1989); by Coulibaly and Shi, 2005).

4.2.4 Annual Maximum Series Derivation

For IDF curve development there are two methods commonly used to extract extreme rainfall data from a time series, which are the annual maximum series (AMS) method and the partial duration series (PDS) method. The AMS method extracts the largest recorded precipitation event from each year. The PDS method sets a precipitation threshold value, i.e. for 24 hour rainfall data, the threshold value can be set to 40 mm (which is site or region dependent), therefore any rainfall event greater than 40 mm will be extracted from the time series and is included when creating IDF curves. There are positive and negative factors associated with both methods. The problem associated with the AMS method is that it only extracts one extreme

rainfall event from a given year, however there may be two or more extreme precipitation events within a year, therefore the extreme rainfall characteristics for a station could be misrepresented. The issue associated with the PDS method is that there is large uncertainty regarding how to properly choose the precipitation threshold value, i.e. is 40 mm more representative of extreme rainfall events than 50 mm. Subjectivity is involved when answering the aforementioned problem. Therefore the AMS method was employed when deriving IDF curves for this study. The AMS data was extracted for all weather stations using MatLab (R2014a).

4.3 At-Site Method IDF Curve Development

The at-site IDF curve method was utilized to develop IDF curves for all weather stations in the study area. Frequency analysis was utilized to determine the recurrence of extreme rainfall events for a variety of return periods. Return periods are measured in years and the range of return periods used in this study include 2, 5, 10, 20, 50 and 100 year return periods. To estimate recurrence intervals of extreme precipitation events a probability distribution was fit to the AMS data. The generalized extreme value (GEV) distribution was the probability distribution function that was chosen based on previous recent study in Southern Ontario (Coulibaly et al., 2015). Once the probability distribution function is fitted to the AMS, estimation of extreme rainfall events for desired return periods can be completed. IDF curves for various storm durations ranging from 15 minutes to 24 hour were created.

4.4 Regional Frequency Analysis Method IDF Curve Development

The regional frequency analysis method was used to create IDF curves for all homogeneous regions identified by selected regionalization techniques. The regional frequency analysis approach includes additional weather stations in the development of IDF curves. Three

clustering techniques were utilized to generate homogeneous regions, which include the Principal Component Analysis (PCA) with k-means, the Ward's method, and the Tabreg approach. A regional probability distribution function was fit to the AMS of all weather stations in each respective cluster. IDF curves for multiple rainfall durations were created for all stations within that cluster.

4.4.1 Regionalization Method Inputs

When using the regional frequency analysis method, it is important to include at-site characteristics as inputs into the clustering technique (Hosking and Wallis, 1997). After completing sensitivity analyses it was determined that the most suitable parameters to characterize precipitation for stations in southern Ontario included mean annual precipitation (MAP), total spring precipitation (April – May), total summer precipitation (June – September), total fall precipitation (October – November), total winter precipitation (December – March) and total 100 maximum daily precipitation values. It is common practice to include input parameters such as number of wet days and elevation, however this is problematic because these aforementioned parameters do not have the same unit so it is difficult to ensure that all of the parameters are evenly weighted. The units for all parameters used in this study are in millimeters. All of the data has been normalized before being inputted into the regionalization techniques.

4.4.2 Principal Component Analysis with K-means Clustering

Principal Component Analysis (PCA) is a multivariate method that discovers patterns and trends within a dataset with the objective of classifying multiple variables using one value (Mallants and Feyen, 1990). In most regionalization studies, multiple variables are assessed to

determine the behavior of a system. PCA extracts information from the original dataset and simplifies it into orthogonal values called principal components (PCs) (Mallants and Feyen, 1990). The first PC explains the largest variance within the dataset, the second PC explains the second largest variance within the dataset, and this trend continues until the last PC is measured (Stathis and Myronidis, 2009). It is acceptable to include PCs where the variance explained is greater than or equal to 80%. PCA was applied to observed data to describe hydrological characteristics of sites located within southern Ontario.

K-means algorithm was used to classify the PCA scores of each weather station into homogeneous regions. K-means algorithm places centroids into a dimension of space which describes the PCA score data (Razavi and Coulibaly, 2013). The Euclidean distance between each cluster centroid and the closest PCA score is measured (Razavi and Coulibaly, 2013). K-means algorithm divides the data into *k* clusters by assigning each PCA score to the respective cluster where the distance between the data point and the cluster centroid is smallest (Fragoso and Tildes Gomes, 2008). The cluster centroids continue to relocate based on the inclusion of data points within each respective cluster. The algorithm continually recalculates the membership of each data point within each cluster in order to obtain new clusters, and this process is carried out until the variance within each cluster is minimized. Therefore each cluster is created based on the minimum Euclidean distance between the cluster centroids and each data point.

The Davies–Bouldin (DB) index introduced by Davies and Bouldin (1979) is a metric for evaluating clustering algorithms. Small values of this index correspond to clusters that are compact (Aguado et al., 2008). Therefore the K-means algorithm with the Davies-Bouldin index is applied to the first two principal components to determine the appropriate number of clusters

for the stations located in the study area (Razavi and Coulibaly, 2013). The number of clusters that minimizes the Davis-Bouldin index is taken as the optimal number of clusters.

4.4.3 Ward's Method

Ward's method is an agglomerative hierarchal clustering technique that was used to group each weather station into clusters that exhibit similar site characteristics. In Ward's method each site behaves as an individual cluster and after each iteration, sites that exhibit the smallest Euclidean distance merge together to form a new cluster. For example, if G_a and G_b are two sites that have the shortest distance between them compared to all other sites, then they merge to form a new cluster $G_{a,b}$ (Kahya et al., 2008). The regionalization process is complete when all sites belong to a single cluster and desired regions are delineated by reducing the variance within each cluster. Hosking and Wallis (1997) recommended using Ward's method for regionalization because it produces adequate clusters with an equal amount of sites in each region.

4.4.4 Tabreg Method

Tabreg was used to cluster weather stations into regions which exbitied similar hydrologic characteristics. The only hard constraint on the formation of regions is that the sites within a region must form a contiguous system. The topology for determining contiguity is provided in Figure 3.

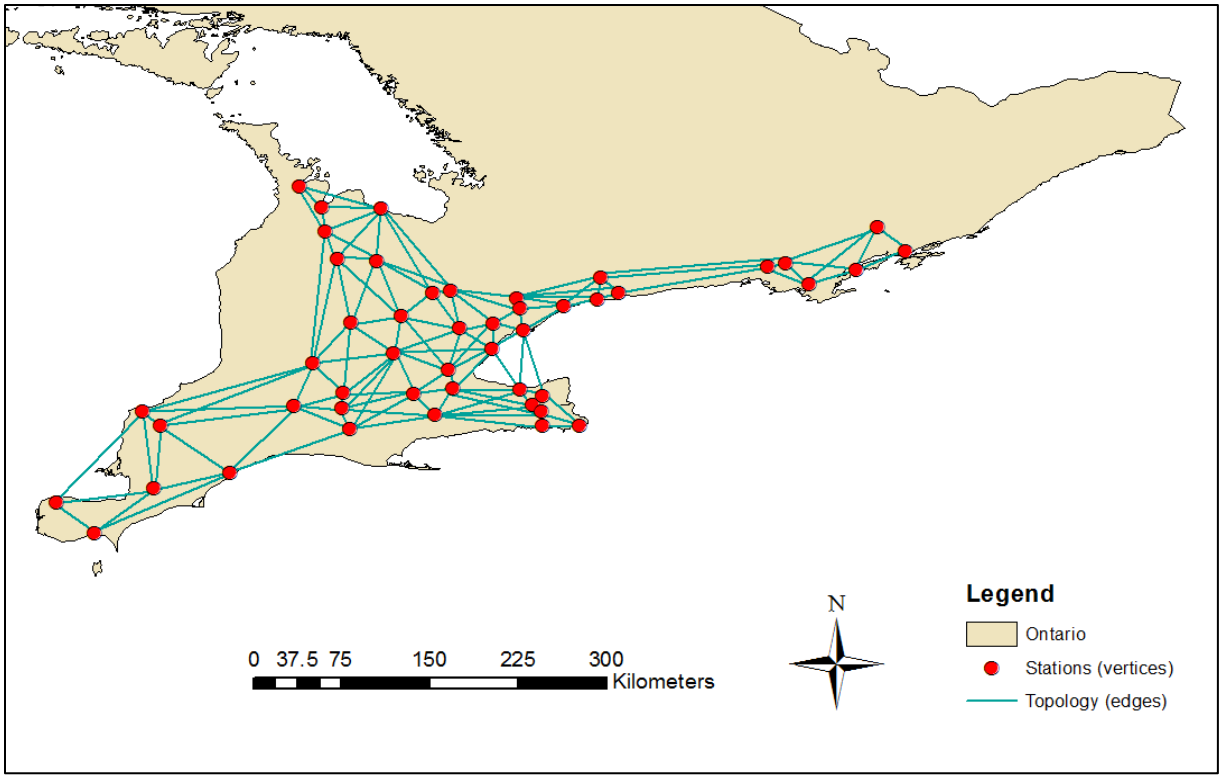

Figure 3: Topology created for the selected weather stations.

In our application, we start with a randomly generated regionalization plan and use Tabreg to search for an improved plan by moving stations between regions in a way that minimizes this cost function subject to the contiguity constraint as follows:

$$C = (V_{x1} + V_{x2} + V_{x3} + V_{x4} + V_{x5} + V_{x6} + V_{x7}) \qquad (3)$$

where C represents the total cost function for the entire regionalization plan, V_{x1} represents the total within-region variation in mean annual precipitation for all sites, V_{x2} represents the total within-region variation in spring precipitation for all sites, V_{x3} represents the total within-region variation in summer precipitation for all sites, V_{x4} represents the total within-region variation in fall precipitation for all sites, V_{x5} represents the total within-region variation in winter

precipitation for all sites, V_{x6} represents the total within-region variation in 100 maximum daily precipitation values for all sites and V_{x7} represents the non-connectivity penalty (Yiannakoulias et al., 2007). The non-connectivity penalty increases the cost associated with regions of irregular shape.

Once an initial randomly generated regionalization plan is found, Tabreg uses a greedy search to move sites into and out of regions in a way that minimizes the cost function. Unfortunately regionalization plans based on greedy searches are not likely to generate good regionalization results. This is because they can get trapped in local (or "poor") optima from which no improved moves can be found. In order to escape poor quality regionalization plans, Tabreg employs a tabu list based on the work of Bozkaya et al. (2003). Local optimum solutions are avoided by memorizing previous station assignments and new regions are created by adding stations into different areas of the search space. This occurs because a tabu list limits certain search options for a period of time. This forces the algorithm to identify new stations that can be added into regions. Initially this can negatively impact the cost functions, however over a long run, as more station assignments are made, the quality of solutions is greatly improved. As displayed in Figure 4, the quality of solutions remains trapped in a local optima for the first 235 iterations. Once the tabu list is activated additional stations are utilized and optimal regions are delineated which is observed when the cost function substantially decreases from 57 to less than 20.

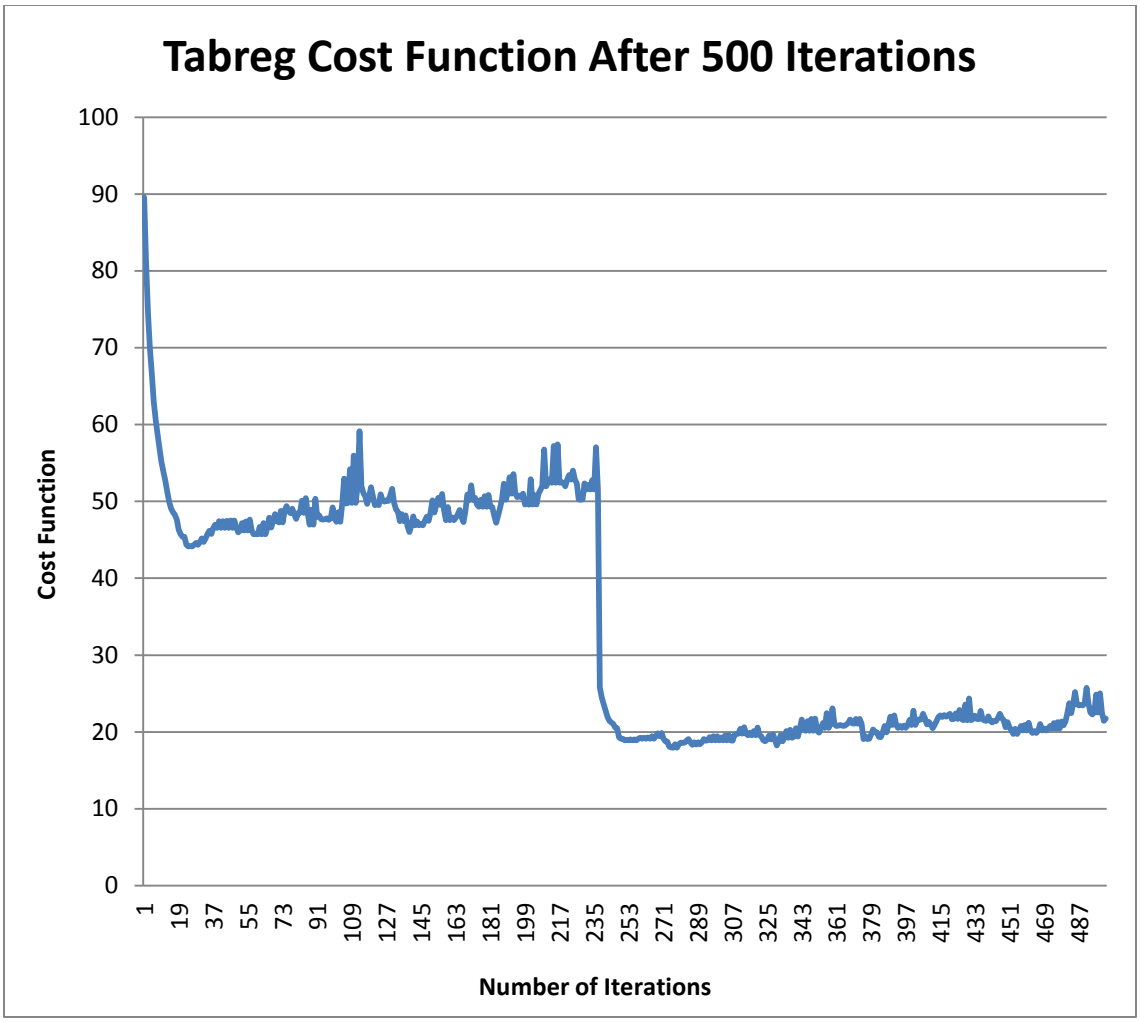

Figure 4: Graphical plot of the cost function after 500 iterations using Tabreg.

A non-connectivity penalty was included in the objective function of the Tabreg method to ensure that regions are relatively compact in shape. Additionally Tabreg ensures that the delineated regions are contiguous, meanwhile PCA with k-means and Ward's method does not ensure this.

4.4.5 L-moments Approach

The L-moments statistics validate the homogeneous regions that are delineated using regionalization techniques. When using this approach it is assumed that stations which form a

homogeneous region represent an identical frequency distribution apart from a site-specific scaling factor (Hosking and Wallis, 1997). The L-moments approach uses multiple datasets from a respective region to compute the final quantile estimates which are used to create regional IDF curves.

4.4.6 L-moment Ratio Diagrams

L-moment ratio diagrams identify the probability distribution function that is most appropriate for each region. The L-moment ratio diagram is used to assess the adequacy of five different three-parameter probability distribution functions for each region, including generalized logistic (GLO), generalized extreme value (GEV), generalized normal (GN), Pearson Type III (P3) and generalized Pareto (GPA) distributions. L-moment ratio diagrams are visual tools which present the L-moment coefficient of kurtosis, τ_4, of each distribution as a function of its L-moment coefficient of skewness, τ_3 (Hosking and Wallis, 1997). For the candidate probability distribution functions, the representation of τ_4 as a function of τ_3 will result in a curve that can be seen on the L-moment ratio diagram (Hosking and Wallis, 1997). In the same diagram the point corresponding to τ_4 as a function of τ_3 for the observed data is considered the reference point. The selection of the best distribution is based on the proximity of the distribution curve in relation to the observed data. A suitable probability distribution function is selected if it is closest to the point of the observed data.

4.4.7 Goodness-of-Fit Measure

When using the L-moment ratio diagram if there are multiple probability distribution functions that are appropriate for a respective region then the goodness-of-fit measure is utilized to accurately determine which probability distribution function is most suitable for each region.

The goodness-of-fit measure assessed the similarity between the sample kurtosis of the observed data and the population kurtosis of the fitted distribution (Hosking and Wallis, 1997). A candidate distribution was selected if the goodness-of-fit measure Z^{DIST} was less than the threshold value 1.64 which corresponds to the 90% normal quantile (Hosking and Wallis, 1997). Z^{DIST} was defined as

$$Z^{DIST} = \frac{\tau_4^{DIST} - \tau_4^R + \beta_4}{\sigma_4} \qquad (4)$$

where *DIST* is any particular candidate distribution that is being assessed, τ_4^R is the regional average L-kurtosis, τ_4^{DIST} is the L-kurtosis of the fitted distribution, β_4 is the bias of the regional average sample L-kurtosis, and σ_4 is the standard deviation of the regional average sample L-kurtosis (Hosking and Wallis, 1997). A candidate distribution was considered satisfactory if $Z^{DIST} \leq 1.64$ and a satisfactory distribution was accepted at a confidence level of 90% (Hosking and Wallis, 1997).

4.5 Future IDF Curve Methodology

4.5.1 Selection of Future Time Periods

Certain climate models do not have the same projected future time periods. In order to allow for a consistent comparison of different climate models, the future time periods for selected climate models must overlap. Two time periods were selected to create future IDF curves for both the CanRCM4-CanESM2 and HadGEM2-ES climate models, the 2050s (2026 – 2045) and the 2100s (2081 – 2099). Both of these time periods follow the RCP4.5 and RCP8.5 scenarios. Therefore for each station, an ensemble of IDF projections were generated using the aforementioned RCP scenarios and future time periods.

4.5.2 Climate Model Data Processing

Data for CanRCM4-CanESM2 was downloaded at the three closest grid points of each station and the inverse distance weighted average was calculated to obtain the daily rainfall data. Data for HadGEM2-ES was downloaded at the closest grid point of each station because GCMs have coarse spatial resolution and only the grid point that is closest to each station can best represent the data. The CanRCM4-CanESM2 data was downloaded in a 1-hour duration format and the HadGEM2-ES data was provided in a 3-hour duration format. In order to obtain climate model data for different storm durations, the aggregation method was applied to the precipitation data to get lower resolution data (i.e. 6-hour, 12-hour and 24-hour for HadGEM2-ES and 3-hour, 6-hour, 12-hour and 24-hour for CanRCM4-CanESM2) and then higher resolution data (i.e. 15-min, 30-min, 1-hour for HadGEM2-ES and 15-min and 30-min for CanRCM4-CanESM2) was derived using the ratio formula presented in *Section 4.1.3* of this study.

4.5.3 Downscaling Techniques

Each climate model scenario is downscaled using a variant of the Delta change method first introduced by Olsson (2009). The Delta change method is a robust downscaling technique that has been implemented by the European Union Sustainable Urban Development Planner for Climate Change Adaptation Project (SUDPLAN, 2012). The Delta change method uses climate projections to estimate the change in current design storms and future design storms and applies this change to historical precipitation data. The projected future design storm I_p is formulated as:

$$I_p = I_o \frac{I_f}{I_c} \qquad (5)$$

where I_f is the future design storm based on future climate model rainfall intensities for a specific duration, I_c is the current design storm based on current climate model rainfall intensities for a specific duration and I_o is the observed rainfall data for a specific duration. The advantage of the Delta change method is that the temporal and spatial variability of the observed data is preserved (Olsson et al., 2009).

4.5.4. Future IDF Curve Derivation

Based on previous recent study (Coulibaly et al. 2015), the generalized extreme value (GEV) distribution was the probability distribution function that was used for all future design storm estimation. IDF curves for each future time period were developed by taking the downscaled output from each climate model and RCP scenario (Coulibaly et al., 2015).

5. Results and Discussion

5.1 Principal Component Analysis and K-means Clustering Regionalization Results

The first step when utilizing regional frequency analysis is determining the number of clusters that are appropriate for the region based on the available data. The k-means algorithm and the Davies-Bouldin index was applied to determine the optimal number of clusters based on the available dataset. The optimal number of clusters equates to the cluster size that has the lowest Davies-Bouldin value. The value of this index is averaged after 10 runs. The results based on the Davies-Bouldin index indicate that nine clusters is appropriate to delineate regions for the sites used in this study (Figure 5).

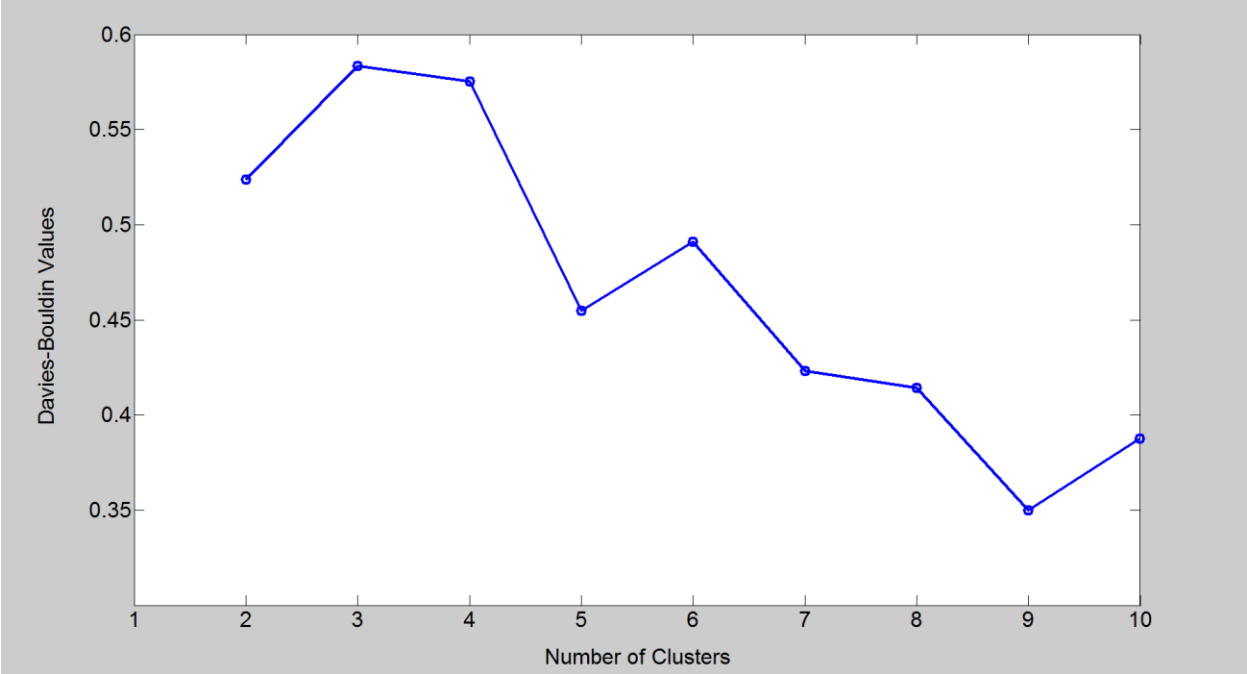

Figure 5: Davies-Bouldin index applied to the input dataset.

The percentage of variability which is explained for each principal component is acceptable at a level of 80%. Figure 6 shows the percentage of variance explained by each principal component. The first two principal components explained approximately 80% of the total variability of the data and will be included in the principal component analysis portion of the study.

The principal component coefficients for each attribute and the principal component scores for each observation are presented in Figure 7. The six parameters are represented as a vector and the position of each vector indicates which parameters influence each principal component. For the first principal component all six parameters have positive coefficients which

indicates that regionalization of the stations will be influenced by all parameters. Mean annual precipitation is the parameter that exhibits the most influence on the first principal component.

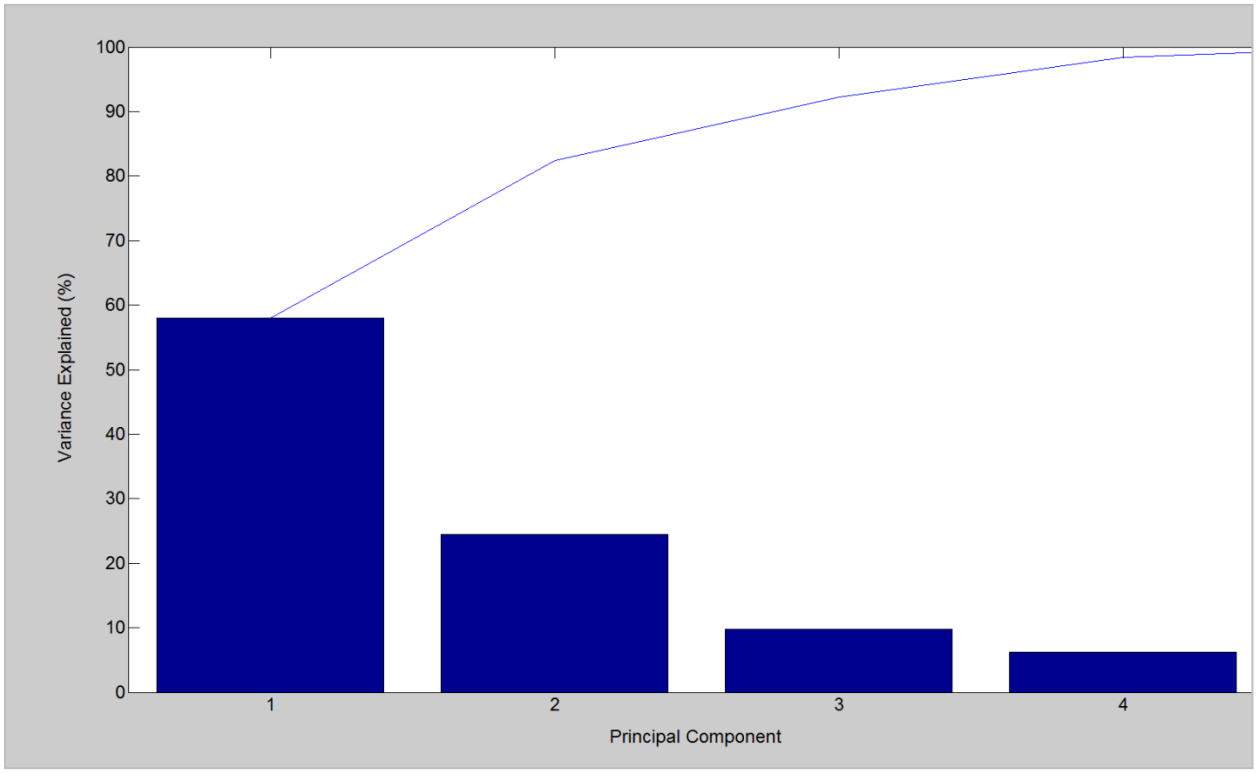

Figure 6: Percentage of total variability explained by each principal component.

Meanwhile total fall precipitation, total winter precipitation, total summer precipitation, total spring precipitation and 100 maximum daily precipitation values have less of an influence on the first principal component (in descending order). The 100 maximum daily precipitation values is the parameter that is represented the most in the second principal component. Total spring precipitation and total summer precipitation are parameters that also exhibited influence on the second principal component. Mean annual precipitation, total fall precipitation and total winter

precipitation are the least influential parameters for the second principal component (in descending order).

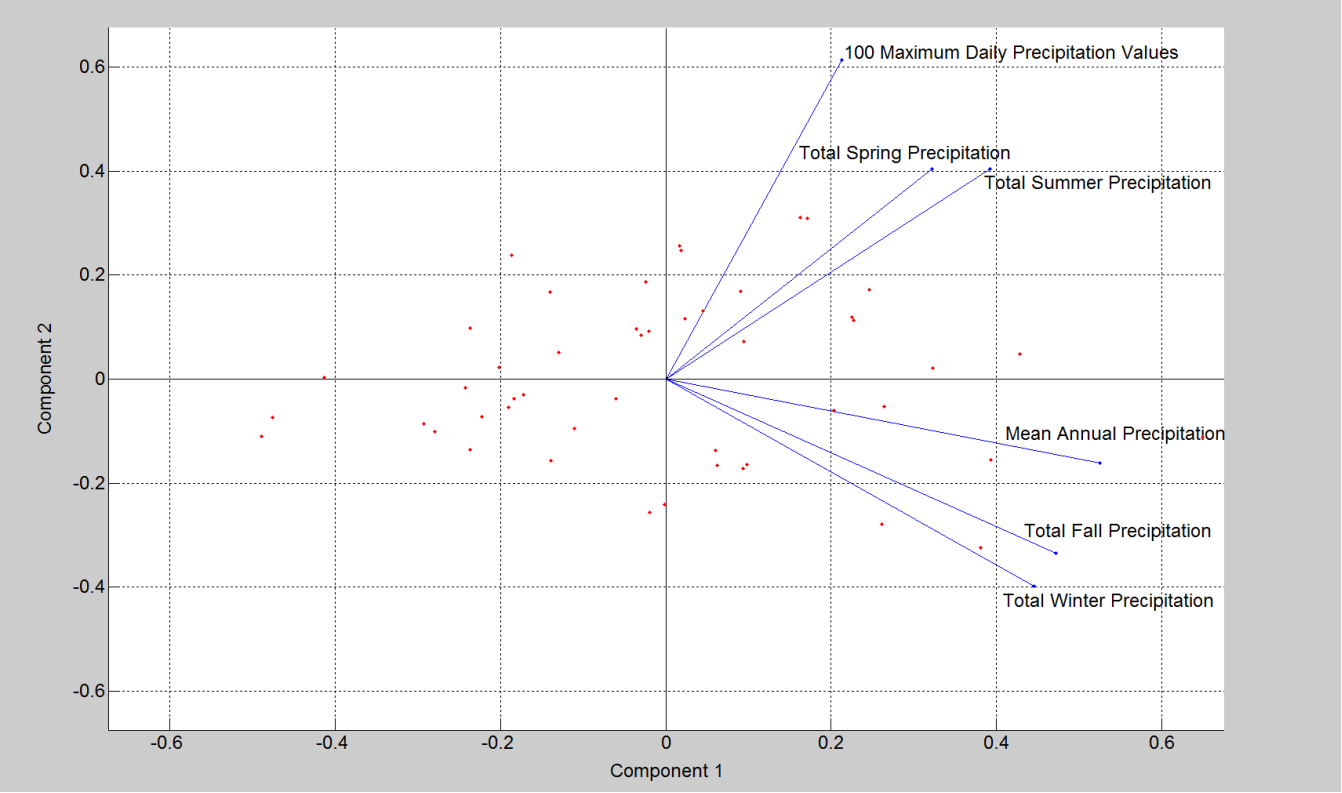

Figure 7: PCA loading plots for the first and second principal components.

The results for weather station regionalization using Principal Component Analysis with k-means clustering are shown in Figure 8. The regionalization results using PCA with k-means clustering show that contiguous homogeneous regions were not obtained and that most regions are heterogeneous. Most clusters contain stations that are located at opposite areas of the study

region. Although some clusters such as cluster 4, cluster 7 and cluster 9 show signs of contiguity it can be seen that the use of PCA with k-means clustering creates heterogeneous regions.

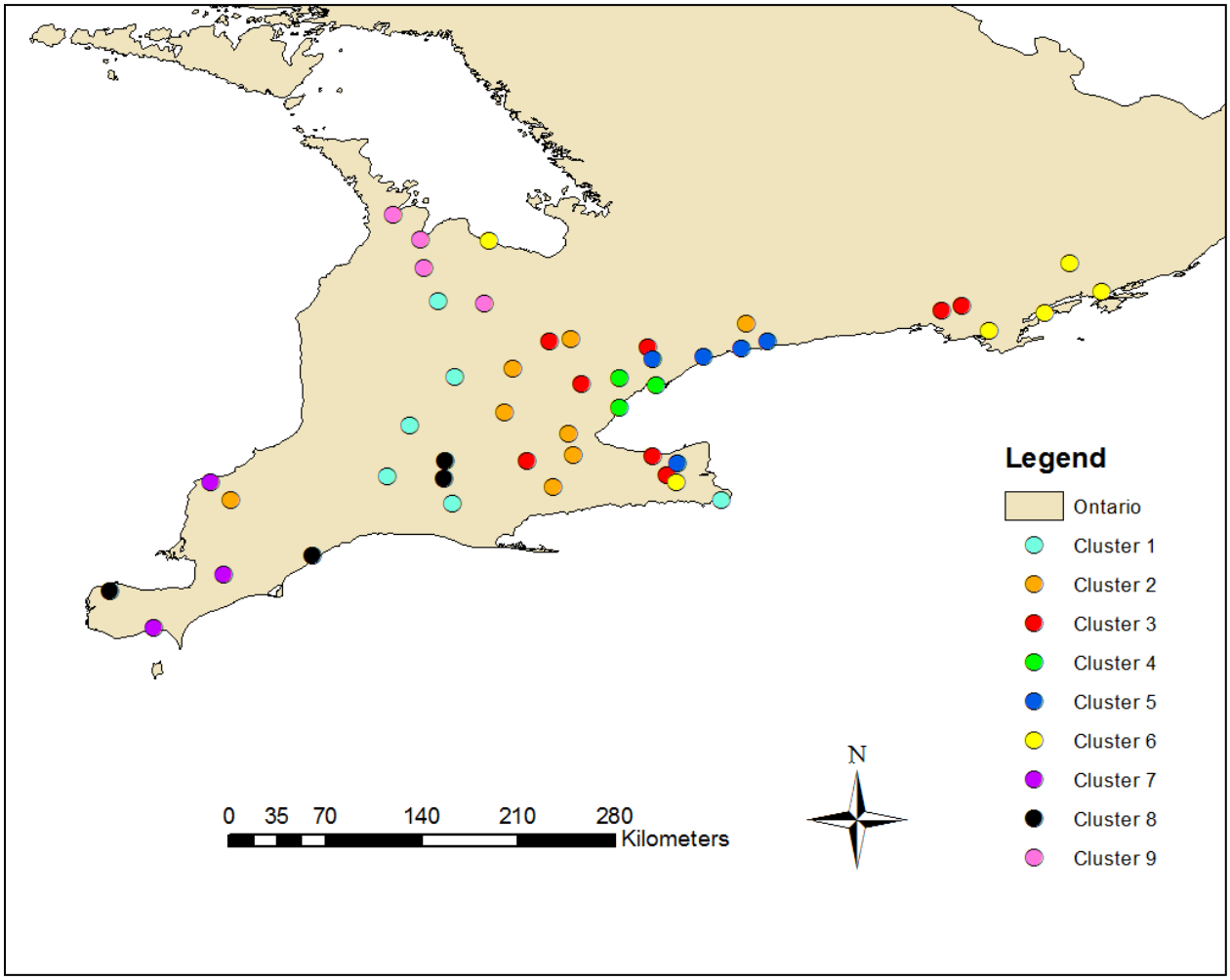

Figure 8: Map showing the regions that were delineated using Principal Component Analysis with k-means.

5.2 Ward's Method Regionalization Results

The results for weather station regionalization using Ward's method are shown in Figure 9. The regions delineated using Ward's method exhibit more contiguity compared to PCA with

k-means clustering, however cluster 1, cluster 2 and cluster 3 show signs of heterogeneity and are not contiguous homogeneous regions (Figure 9). However, the method also delineated contiguous homogeneous: cluster 4, cluster 6, cluster 9 and cluster 9. But, most regions created using Ward's method are heterogeneous.

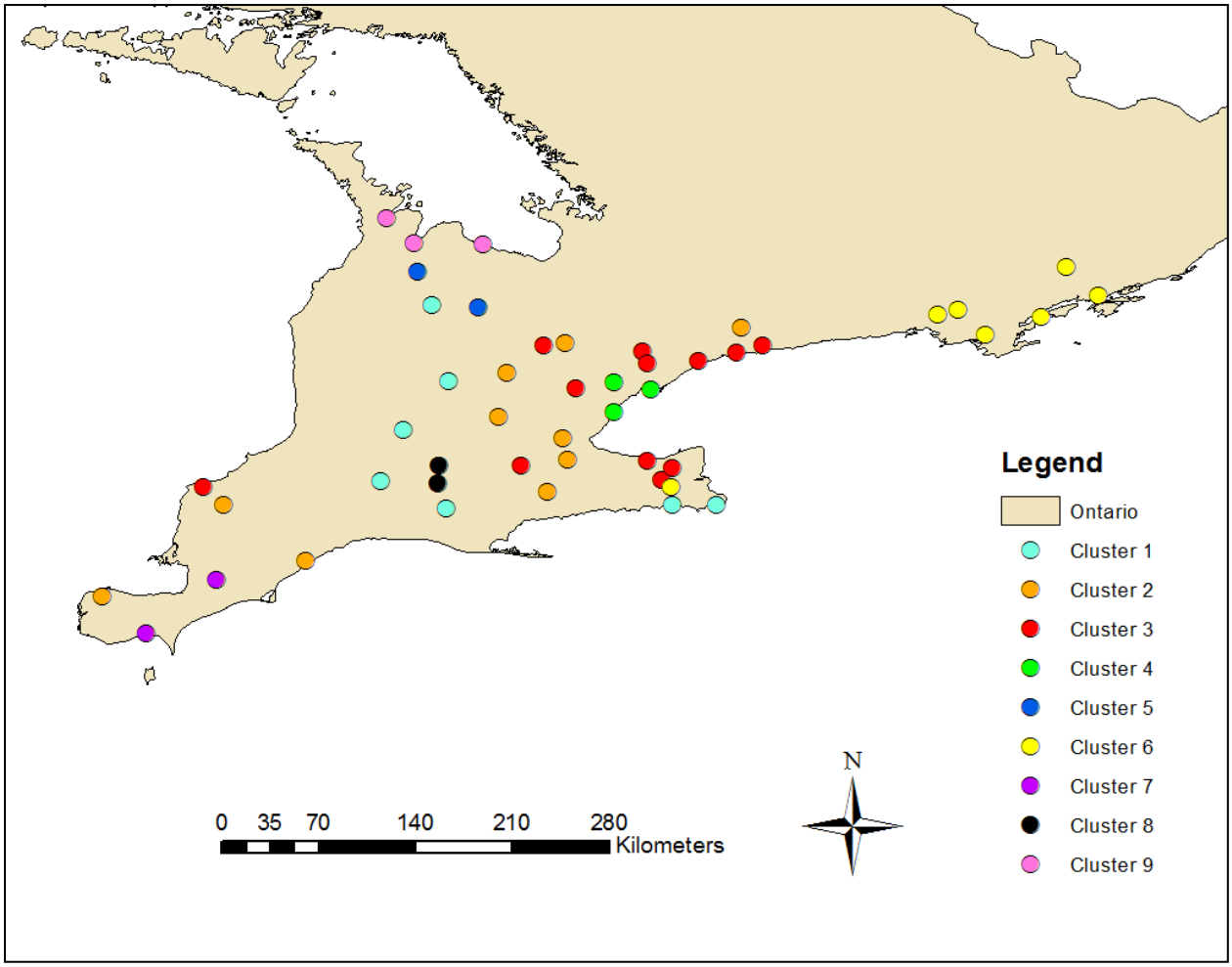

Figure 9: Map showing the regions that were delineated using Ward's method.

PCA with k-means clustering and Ward's method produced clusters that are not contiguously homogeneous. An important aspect of regional frequency analysis is to delineate contiguous homogeneous regions. In previous studies it is common to see methods such as PCA with k-means clustering and Ward's method to include input parameters such as latitude and

longitude which allow for the delineation of contiguous regions. Initially latitude and longitude were not included as input parameters for this study. Additional tests were completed where latitude and longitude were included as input parameters however this did not obtain better results as the new regions that were created still did not exhibit contiguity. Therefore the inclusion of a regionalization technique that accounts for contiguity and is able to cluster the stations into statistically homogeneous regions is required. Tabreg clustering method has proven to be a robust method that accounts for contiguity and it was used as an additional regionalization method.

5.3 Tabreg Regionalization Results

The Tabreg clustering method was used to delineate homogeneous regions and the results show that the clusters that were formed are uniformly and contiguously regionalized (Figure 10).

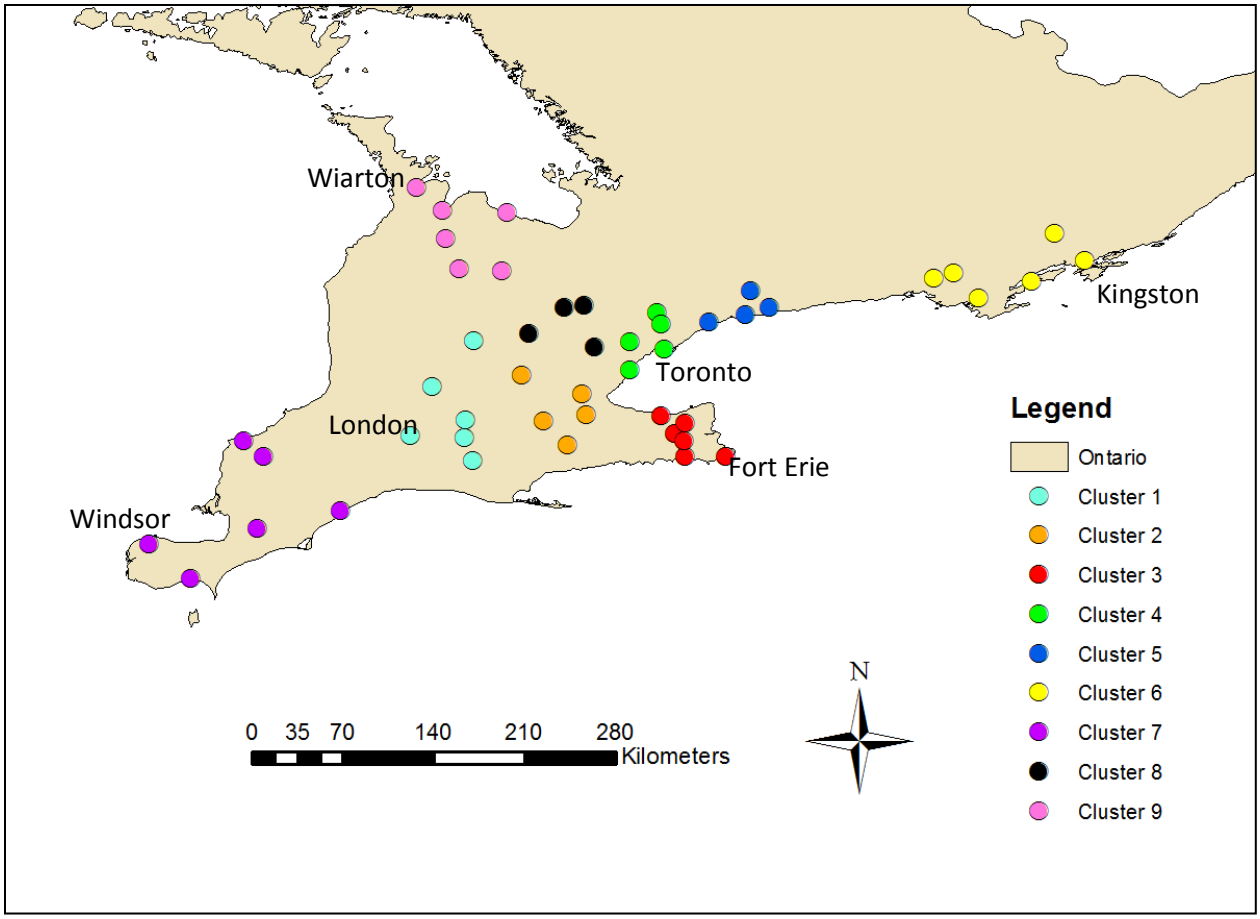

Figure 10: Map showing the regions that were delineated using Tabreg clustering method.

Therefore the regions delineated using the Tabreg method will be used for regional frequency analysis in this study. To ensure that the clusters are statistically homogeneous the L-moments approach was applied to each cluster delineated using Tabreg. All of the clusters obtained using Tabreg successfully passed the discordancy measure and the heterogeneity measure test.

5.4 L-moment ratio diagrams

L-moment ratio diagrams are visual tools that assess which probability distribution functions are most appropriate for each clusters' dataset. The probability function closest to the reference point (the + symbol in Figure 11 and Figure 12) is considered the most appropriate

function. The most appropriate probability distribution function that will be used for cluster 1 is the generalized logistic (GLO) probability distribution (Figure 11) and for cluster 2 it is the generalized extreme value (GEV) probability distribution (Figure 12).

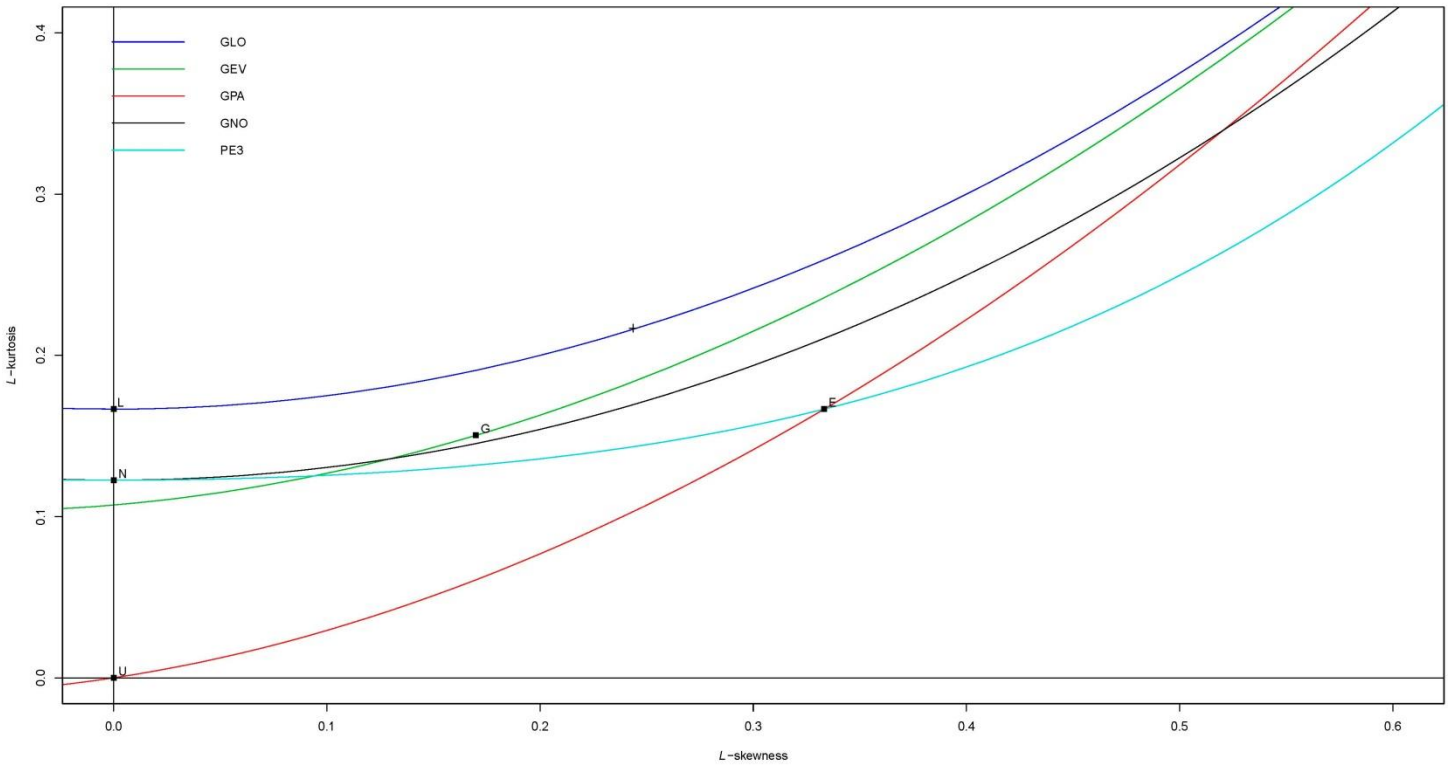

Figure 11: L-moment ratio diagram for cluster 1. *Note:* Each line on the graph represents different three-parameter distributions that were tested for cluster 1. The three-parameter distributions used are: GPA: Generalized Pareto, GEV: Generalized Extreme Value, GLO: Generalized Logistic, LN3: Lognormal and PE3: Pearson Type 3; the + symbol is the reference point; the ■ symbol represents the different two-parameter distributions that were tested for cluster 1. The two-parameter distributions used are E: Exponential, G: Gumbel, L: Logistic, N: Normal and U: Uniform.

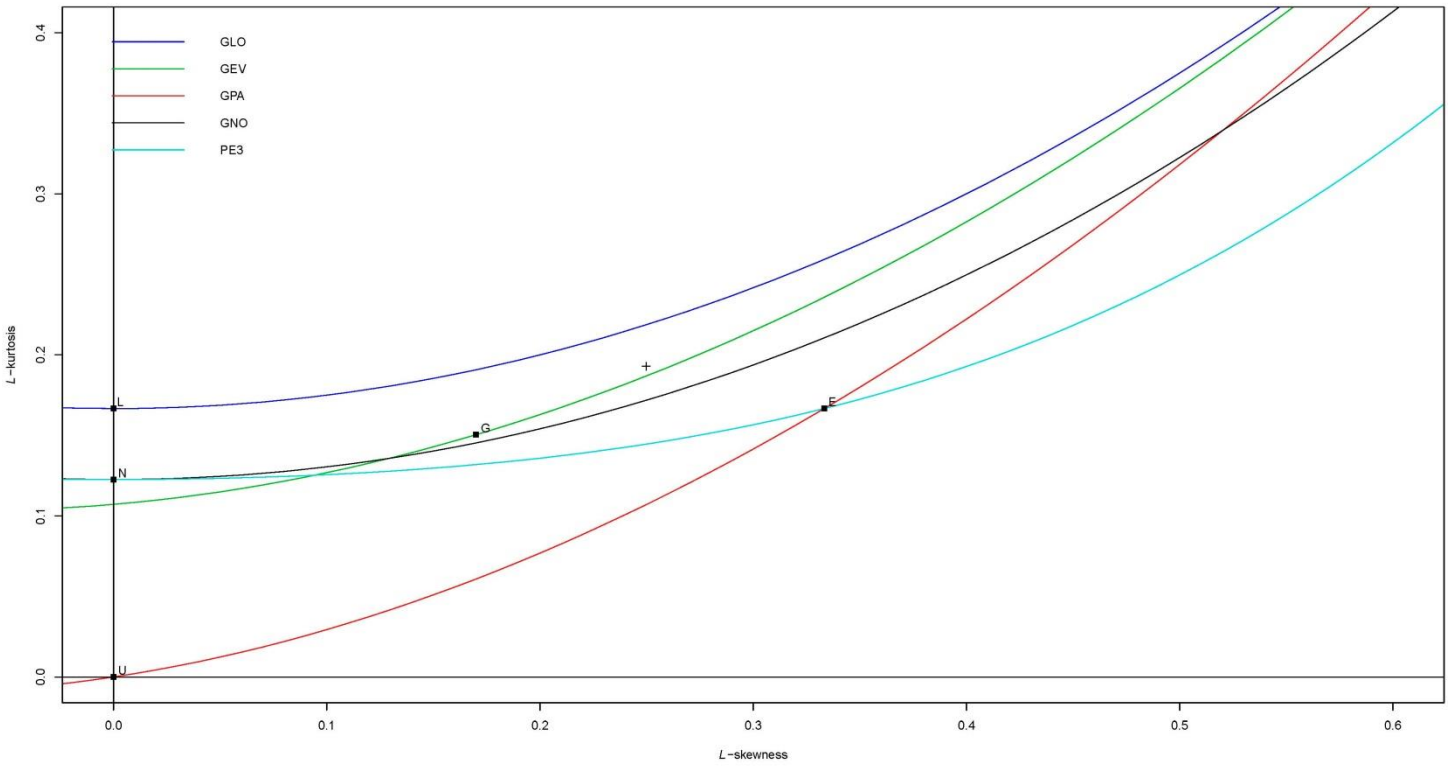

Figure 12: L-moment ratio diagram for cluster 2. *Note:* Each line on the graph represents different three-parameter distributions that were tested for cluster 2. The three-parameter distributions used are: GPA: Generalized Pareto, GEV: Generalized Extreme Value, GLO: Generalized Logistic, LN3: Lognormal and PE3: Pearson Type 3; the + symbol is the reference point; the ■ symbol represents the different two-parameter distributions that were tested for cluster 2. The two-parameter distributions used are E: Exponential, G: Gumbel, L: Logistic, N: Normal and U: Uniform.

5.5 Goodness-of-fit measure

The goodness-of-fit measure was utilized to confirm the most appropriate regional probability distribution function for each cluster. There are many cases where more than one probability distribution appropriately fits the dataset. For cluster 1 there are three probability distributions that can appropriately fit the cluster's dataset, including the generalized logistic distribution, generalized extreme value distribution and generalized normal distribution (Table 2). For cluster 2 there are four probability distributions that can appropriately fit the cluster's data (Table 3). Since multiple probability distributions passed the goodness-of-fit measure, the Z^{DIST} score closest to 0 is used to determine the most suitable probability distribution for each cluster. The most suitable probability distributions for all clusters can be found in Table 4.

Cluster 1	
Probability Distribution Function	Goodness-of-fit measure
Generalized Logistic	-0.39
Generalized Extreme Value	-1.18
Generalized Normal	-1.52

Table 2: Goodness-of-fit measure results for each station located in cluster 1.

Cluster 2	
Probability Distribution Function	Goodness-of-fit measure
Generalized Logistic	0.50
Generalized Extreme Value	-0.32
Generalized Normal	-0.71
Pearson Type III	-1.42

Table 3: Goodness-of-fit measure results for each station located in cluster 2.

Cluster Identification	Best Fit Distribution
Cluster 1	GLO
Cluster 2	GEV
Cluster 3	GEV
Cluster 4	GNO
Cluster 5	GLO
Cluster 6	GPA
Cluster 7	PE3
Cluster 8	GPA
Cluster 9	GNO

Table 4: L-moment ratio diagram results for each cluster.

5.6 IDF Curve Results: At-Site Method Compared to Regional Frequency Analysis Method

After determining the most appropriate regional probability distribution function for each cluster, IDF curves were created for each station using multiple return periods. For illustrative purposes, the at-site method (following the GEV distribution) and the regional frequency analysis method IDF curve results were compared for selected stations in different clusters. The at-site IDF curve and the regional frequency analysis method IDF curve for Glen Allen station are shown in Figure 13. The at-site IDF curve and the regional frequency analysis method IDF curve for Tillsonburg station are shown in Figure 14. Glen Allen and Tillsonburg are located in cluster 1 and the probability distribution function that is used for regional frequency analysis for cluster 1 is the generalized logistic distribution. For the 3 hour and 12 hour duration rainfall the at-site method produces similar rainfall values compared to the regional frequency analysis method for the 2, 5 and 10 year return period for both Glen Allen station (Figure 13) and Tillsonburg station (Figure 14). The regional frequency analysis method produces slightly larger rainfall values compared to the at-site method for the 20 year return period for Glen Allen and Tillsonburg. For the 50 year and 100 year return period the regional frequency analysis method produces significantly larger rainfall values compared to the at-site method for Glen Allen and Tillsonburg.

Using two different probability distribution functions for the at-site IDF curve and the regional frequency analysis IDF curve contributed to the differences that were observed between the at-site method and the regional frequency analysis method. The Z-score probability values for the generalized logistic distribution and the Z-score probability values for the generalized extreme value distribution are similar for the 2, 5 and 10 year return periods. However for the

larger return periods – such as 20, 50 and 100 years – the generalized logistic and the generalized extreme value distributions have large differences in Z-score probability values. Since the Z-score probability values for short return periods are similar for both the GEV and GLO distributions then the IDF curve values are also similar. However for the larger return periods, the GLO Z-score probability values are larger compared to the GEV Z-score probability values and as a result the final IDF curve values for the regional frequency analysis method are subsequently larger than the rainfall values of the at-site method. There are other clusters in the study area that have a different regional probability distribution function compared to the at-site probability distribution. As a result significant differences of rainfall values were observed for larger return periods in other clusters as well. The patterns observed using the at-site method and regional frequency analysis method are displayed by showing the percentage difference of the rainfall intensities produced for the at-site method and the regional frequency analysis method (Figure 15).

(a) *(b)*

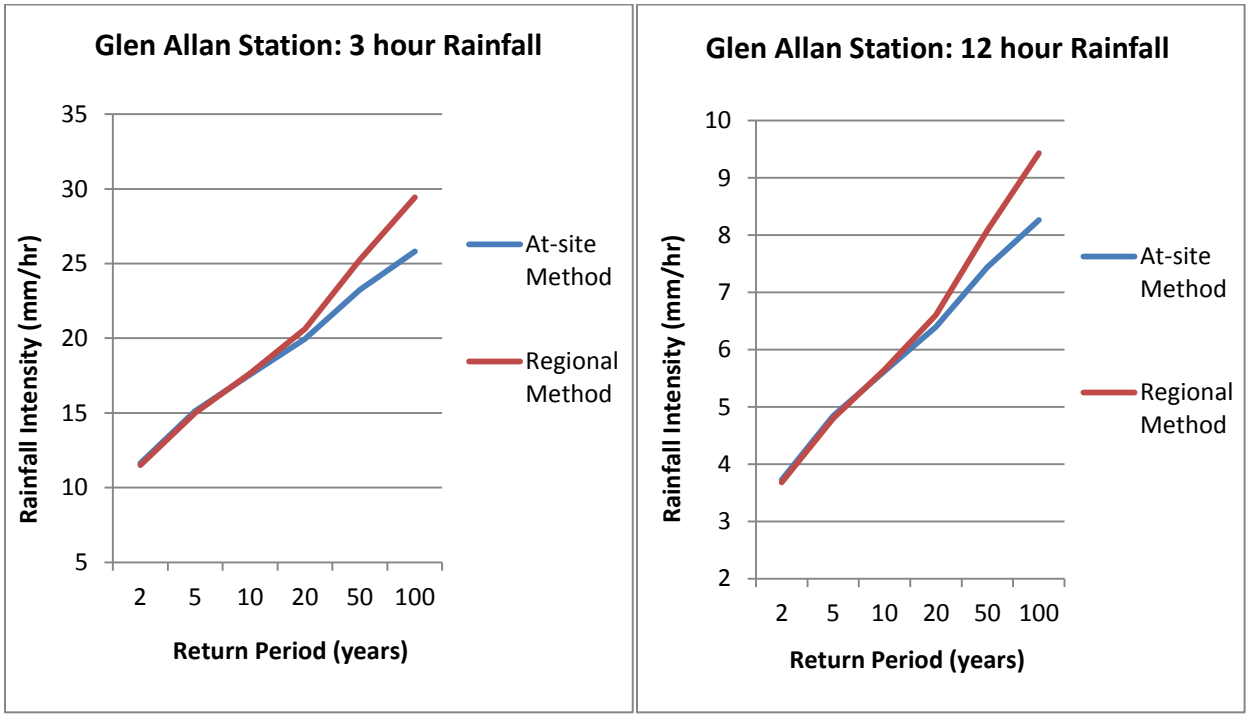

Figure 13: Plots of IDF statistics from the regional frequency analysis method and the at-site method for Glen Allan station (cluster 1): *(a)* 3 hour rainfall and *(b)* 12 hour rainfall.

(a) *(b)*

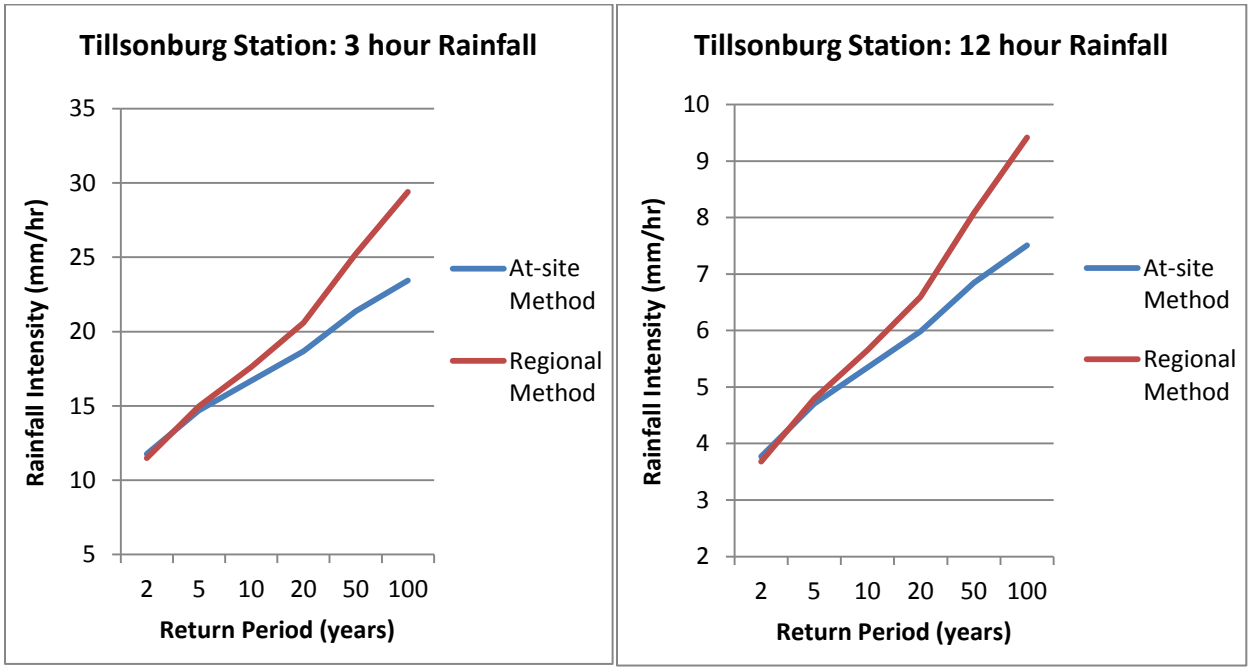

Figure 14: Plots of IDF statistics from the regional frequency analysis method and the at-site method for Tillsonburg station (cluster 1): *(a)* 3 hour rainfall and *(b)* 12 hour rainfall.

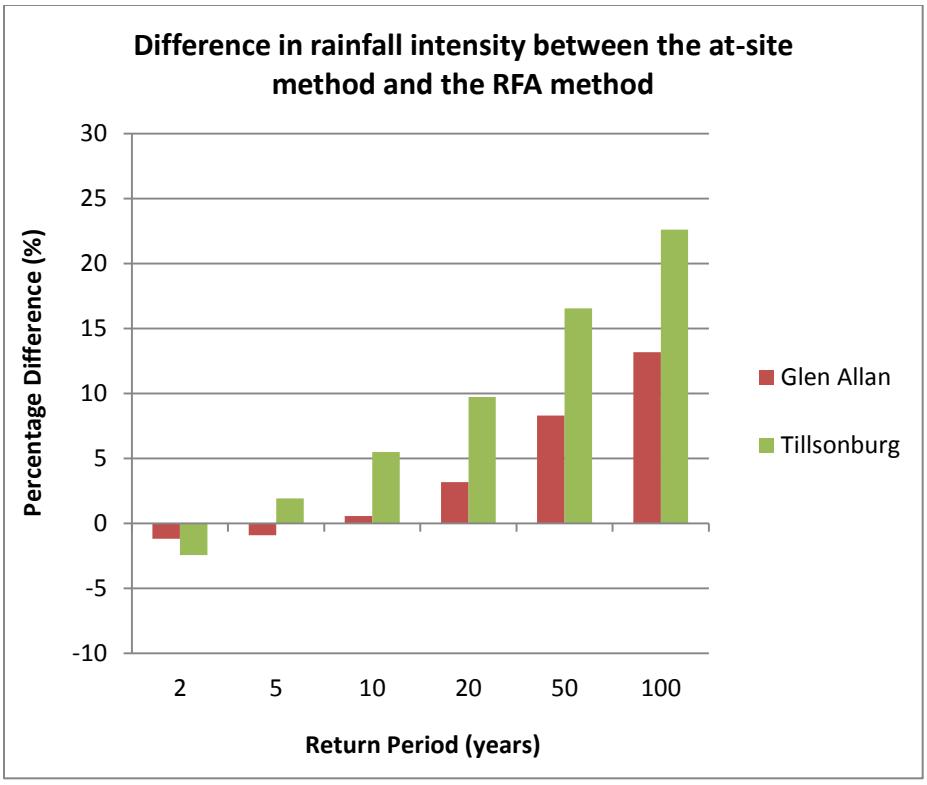

Figure 15: Difference (*in %*) of rainfall intensity between the at-site method and the regional frequency analysis method for stations in cluster 1.

After comparing IDF curves using the at-site method and the regional frequency analysis method with different probability distribution functions, the differences in rainfall values for larger return periods were obvious. Given that certain clusters use the GEV distribution similarly to the at-site method, the next set of stations compared using the at-site method and the regional frequency analysis method will use the GEV distribution to see if there are still differences in final IDF values. The at-site IDF curve and the regional frequency analysis method IDF curve for Vineland Rittenhouse station are shown in Figure 16. The at-site IDF curve and the regional frequency analysis method IDF curve for Hagersville station are shown in Figure 17. Vineland

Rittenhouse is located in cluster 3 and Hagersville is located in cluster 2 and the probability distribution function that is used for regional frequency analysis for cluster 2 and cluster 3 is the generalized extreme value (GEV) distribution also used for all stations in the at site method. For the 3 hour and 12 hour duration rainfall, the at-site method produces similar rainfall values compared to the regional frequency analysis method for the 2, 5 and 10 year return period for both Vineland Rittenhouse (Figure 16) and Hagersville (Figure 17). The regional frequency analysis method produces slightly larger rainfall values compared to the at-site method for the 20 year return period for Vineland Rittenhouse (Figure 16), however the regional frequency analysis method has similar rainfall values as the at-site method at the 20 year return period for Hagersville (Figure 17). For the 50 year and 100 year return period the regional frequency analysis method produces larger rainfall values compared to the at-site method for Vineland Rittenhouse and Hagersville.

A similar trend that was observed in the cluster 1 results is also observed in the results for cluster 2 and cluster 3 where the rainfall values for the at-site method and the regional frequency analysis method are similar for the 2, 5 and 10 year return period. However for the larger return periods – including 20, 50 and 100 years – the rainfall values are larger for the regional frequency analysis method compared to the at-site method. Therefore the final IDF values for the at-site method are similar to the regional frequency analysis method for short return periods for both stations. The patterns observed using the at-site method and regional frequency analysis method are displayed by showing the percentage difference of the rainfall intensities produced for the at-site method and the regional frequency analysis method (Figure 18).

(a) *(b)*

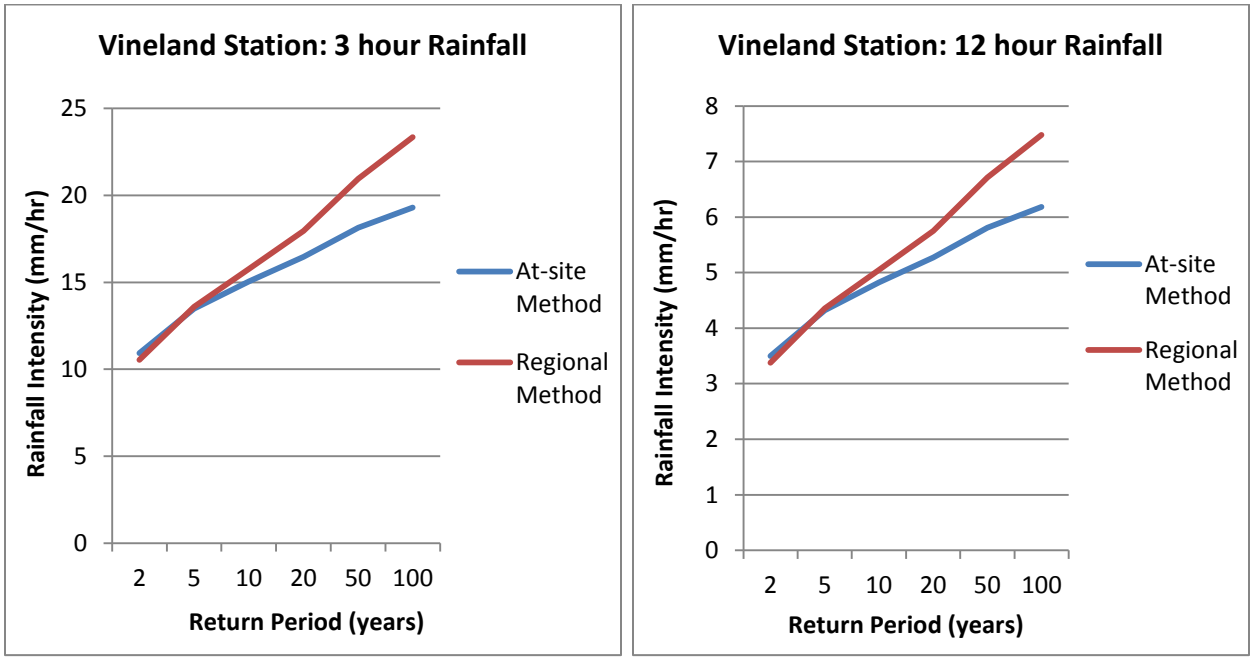

Figure 16: Plots of IDF statistics from the regional frequency analysis method and the at-site method for Vineland Rittenhouse station (cluster 3): *(a)* 3 hour rainfall and *(b)* 12 hour rainfall.

(a) *(b)*

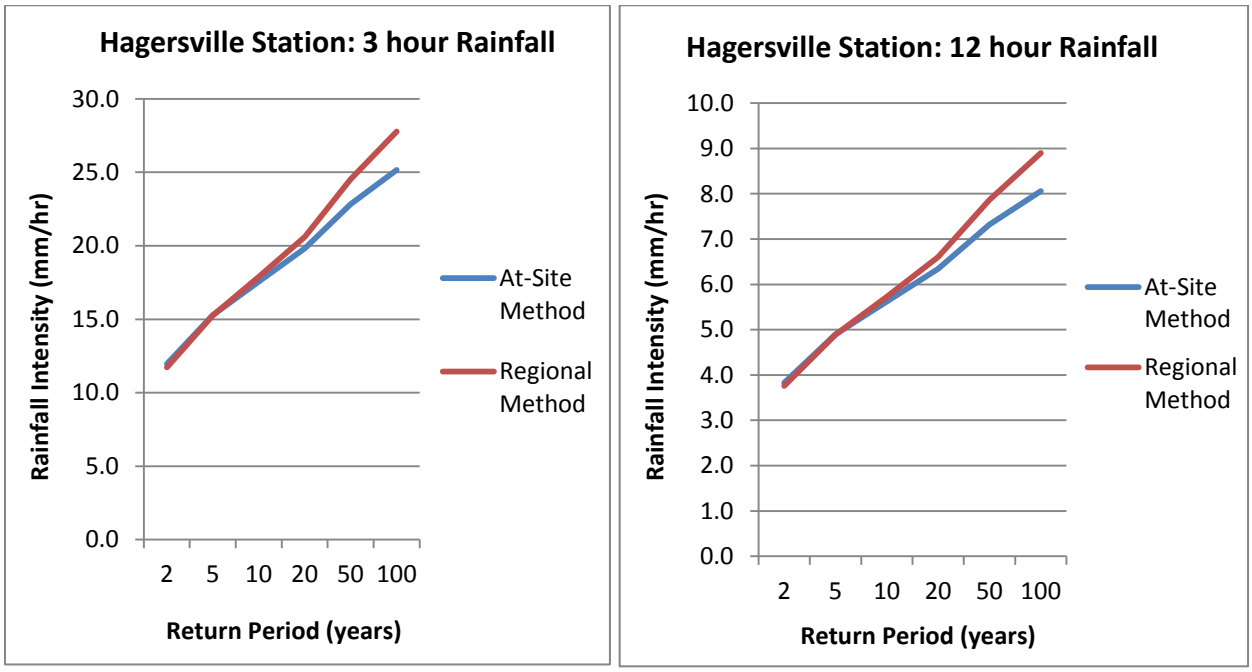

Figure 17: Plots of IDF statistics from the regional frequency analysis method and the at-site method for Hagersville station (cluster 2): *(a)* 3 hour rainfall and *(b)* 12 hour rainfall.

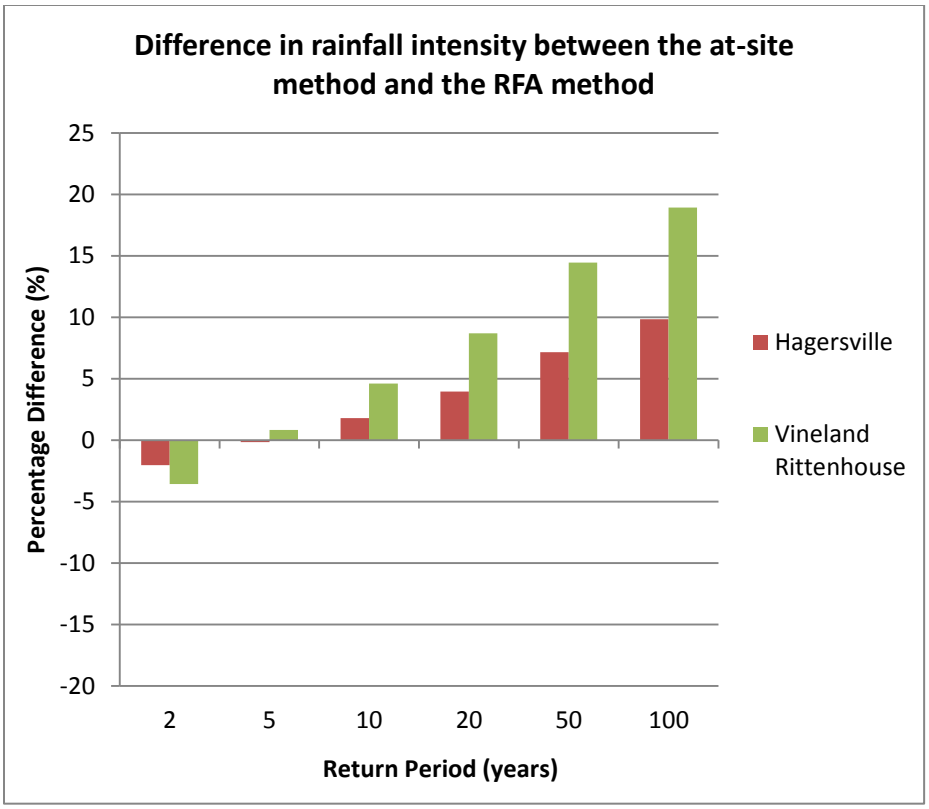

Figure 18: Difference (*in %*) of rainfall intensity between the at-site method and the regional frequency analysis method for Hagersville (cluster 2) and Vineland Rittenhouse (cluster 3).

Furthermore, the at-site method and the regional frequency analysis method were compared using weather stations from all clusters for short return periods (Figure 19) and for large return periods (Figure 20). Similar trends that were observed in clusters 1, 2 and 3 are also found within the other delineated clusters as differences in rainfall intensities for large return periods are obvious, however for short return periods rainfall values are similar. Cluster 2 and cluster 3 use the generalized extreme value as the regional probability distribution, and the regional frequency analysis method produces larger rainfall values compared to the at-site

method. Meanwhile clusters 1, 4, 5, 6, 7, 8 and 9 use a different regional probability distribution compared to the at-site method, and differences in rainfall values are observed for larger return periods as well. Overall using the regional frequency analysis method produces differences in rainfall values compared to the at-site method, especially for large return periods. Similar patterns are observed for clusters where the regional frequency analysis probability distribution and the at-site probability distribution are different or identical. There were also cases where stations using the at-site method produced larger rainfall values compared to the regional frequency analysis method. Therefore regardless of which probability distribution function is used for each IDF method, the IDF values are generally different for larger return periods (50 to 100 years).

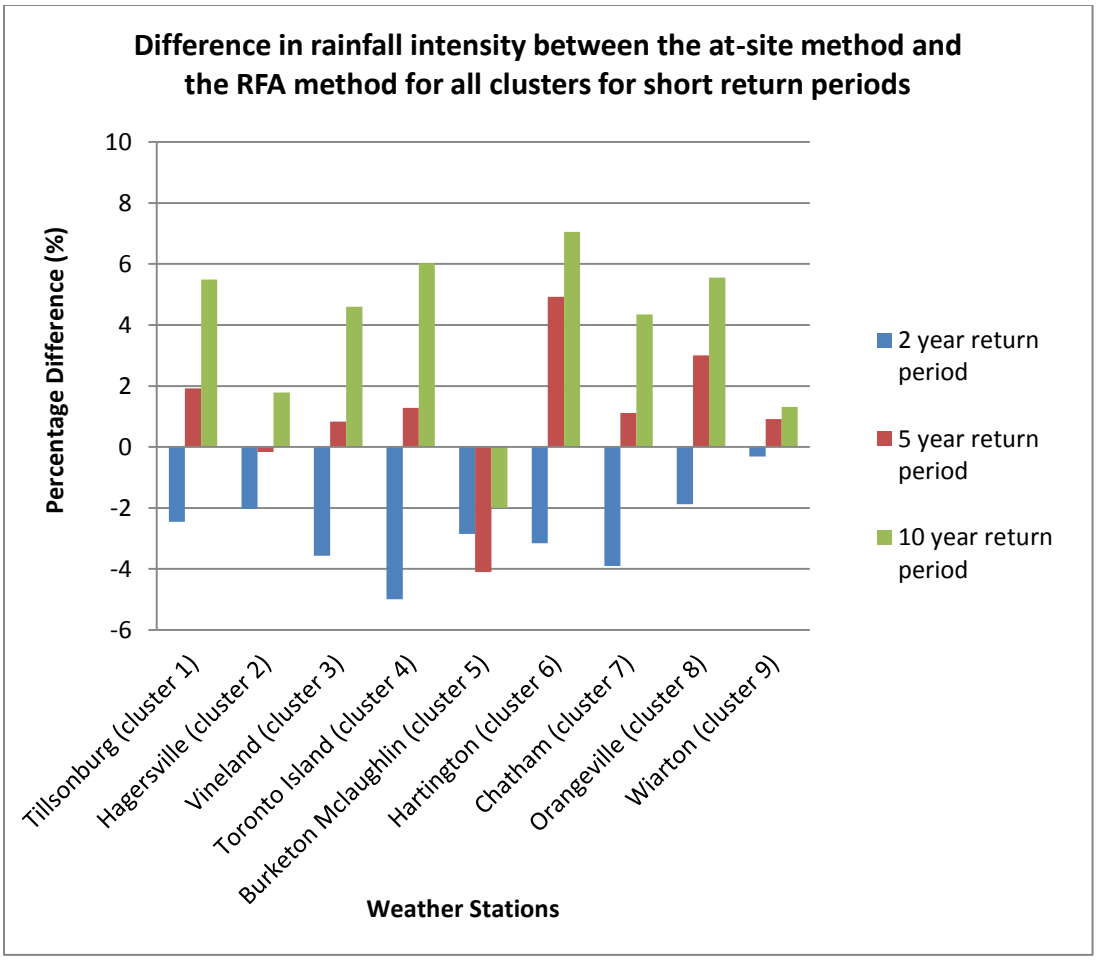

Figure 19: Difference (*in %*) of rainfall intensity between the at-site method and the regional frequency analysis method for weather stations in all clusters for short return periods.

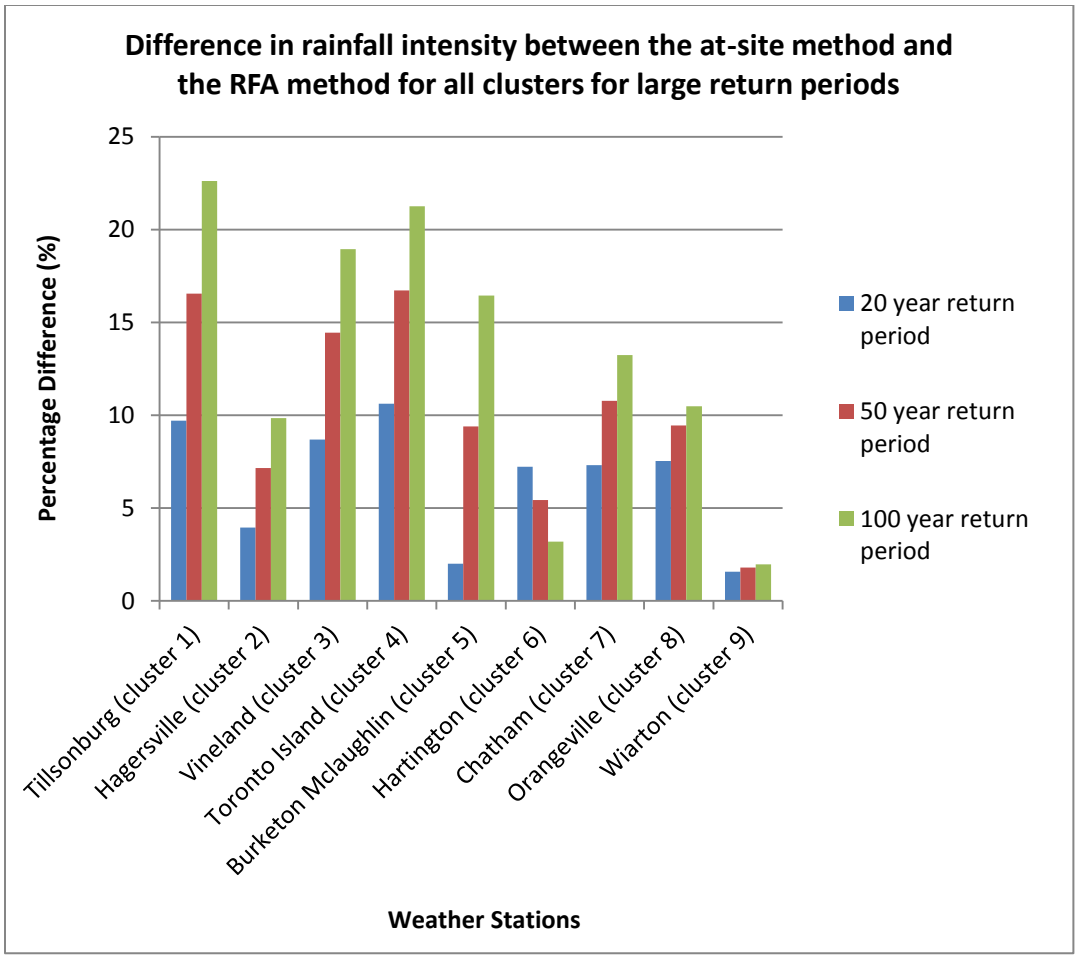

Figure 20: Difference (*in %*) of rainfall intensity between the at-site method and the regional frequency analysis method for weather stations in all clusters for large return periods.

5.7 Future IDF Curve Results

To simplify results presentation, sample station results are presented for illustration. Durham station is located in cluster 9 and Hartington station is located in cluster 6 and despite being at large distance away from one another, similar future IDF curve results were observed for both stations. Figure 19 shows the future IDF results for Durham station for the 3 hour

rainfall duration and Figure 20 shows the Durham station results for the 12 hour rainfall duration. Figure 21 shows the future IDF curves for Hartington station for the 3 hour rainfall duration and Figure 22 shows the Hartington station results for the 12 hour rainfall duration. Future IDF curves derived for the 2050s period and 2100s period were compared with the IDF curve results using the at-site method and the regional frequency analysis method. The 2050s period has larger rainfall values compared to the at-site method and the regional frequency analysis method for all return periods for both Durham (Figure 19 and Figure 20) and Hartington (Figure 21). However for the 12 hour duration for Hartington station, the regional frequency analysis method has larger rainfall values for the 10, 20, 50 and 100 year return period compared to the 2050s period (Figure 22 *a*). The 2100s period has significantly larger rainfall values compared to the 2050s period, the at-site method and the regional frequency analysis method for all return periods for Durham station and Hartington station.

(a) *(b)*

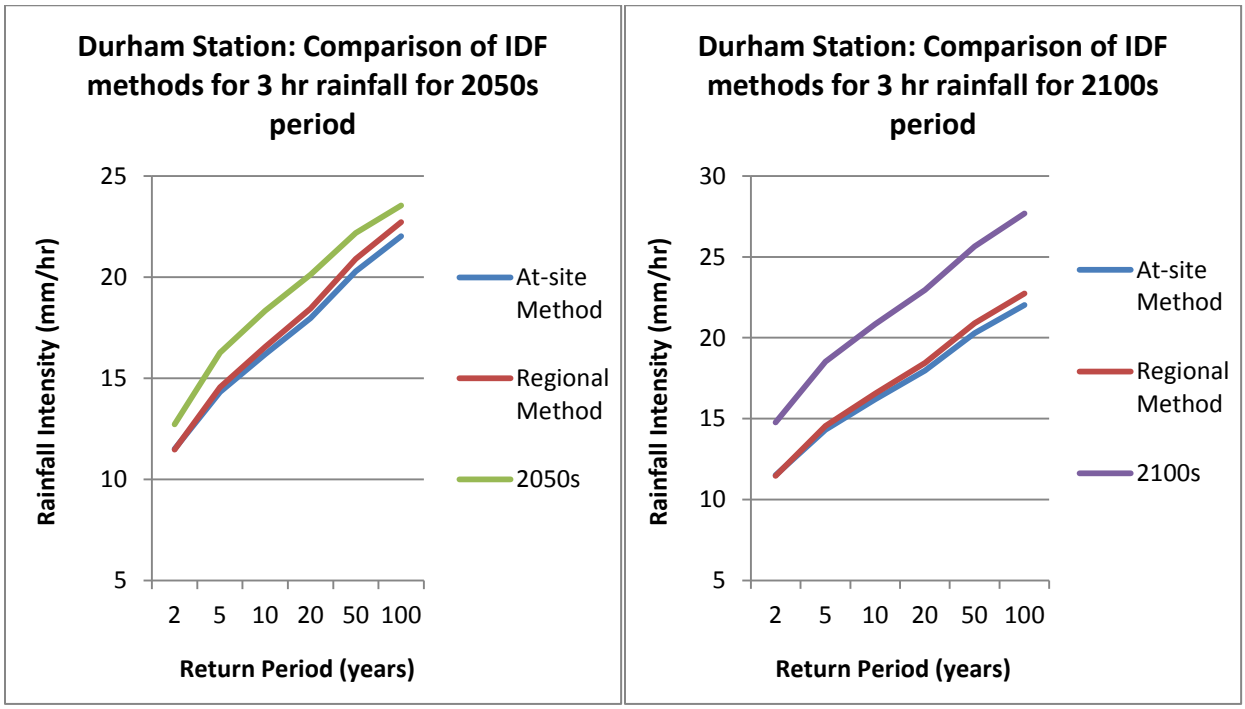

Figure 21: IDF curves obtained from the future IDF method, the regional frequency analysis method and the at-site method for Durham station (cluster 9) for the 3 hour rainfall: *(a)* 2050s period and *(b)* 2100s time period.

(a) *(b)*

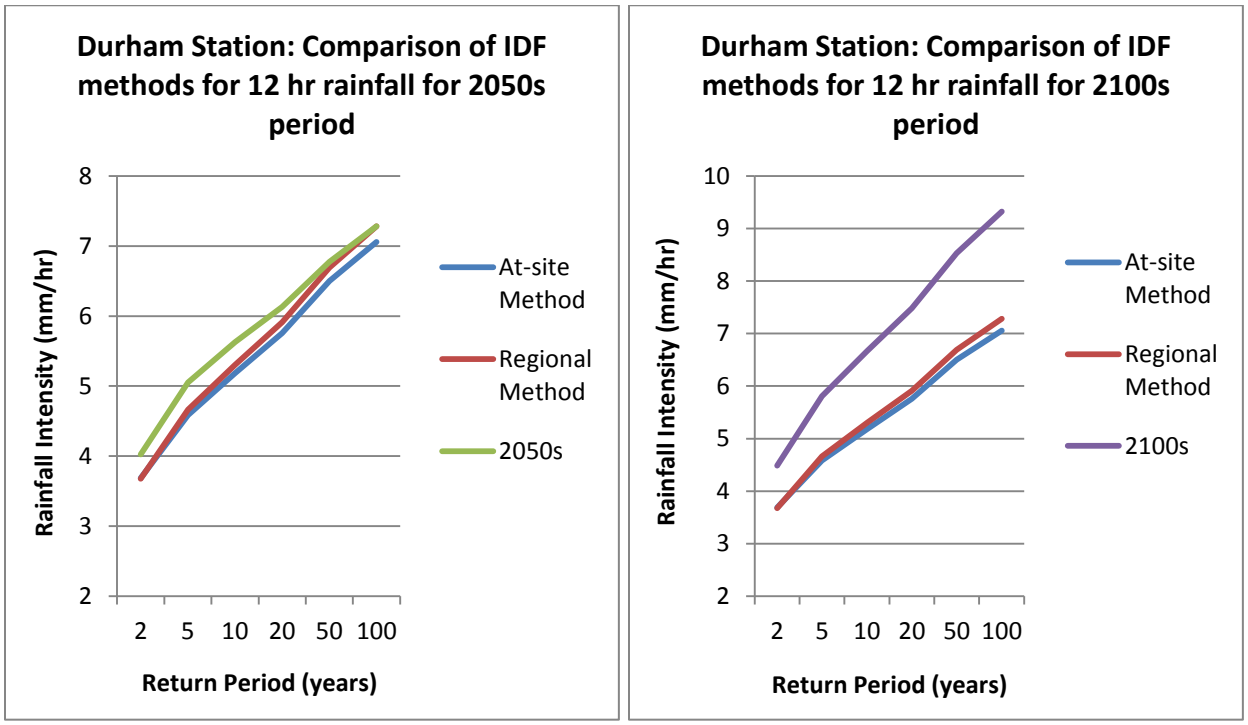

Figure 22: IDF curves obtained from the future IDF method, the regional frequency analysis method and the at-site method for Durham station (cluster 9) for the 12 hour rainfall: *(a)* 2050s period and *(b)* 2100s time period.

(a) *(b)*

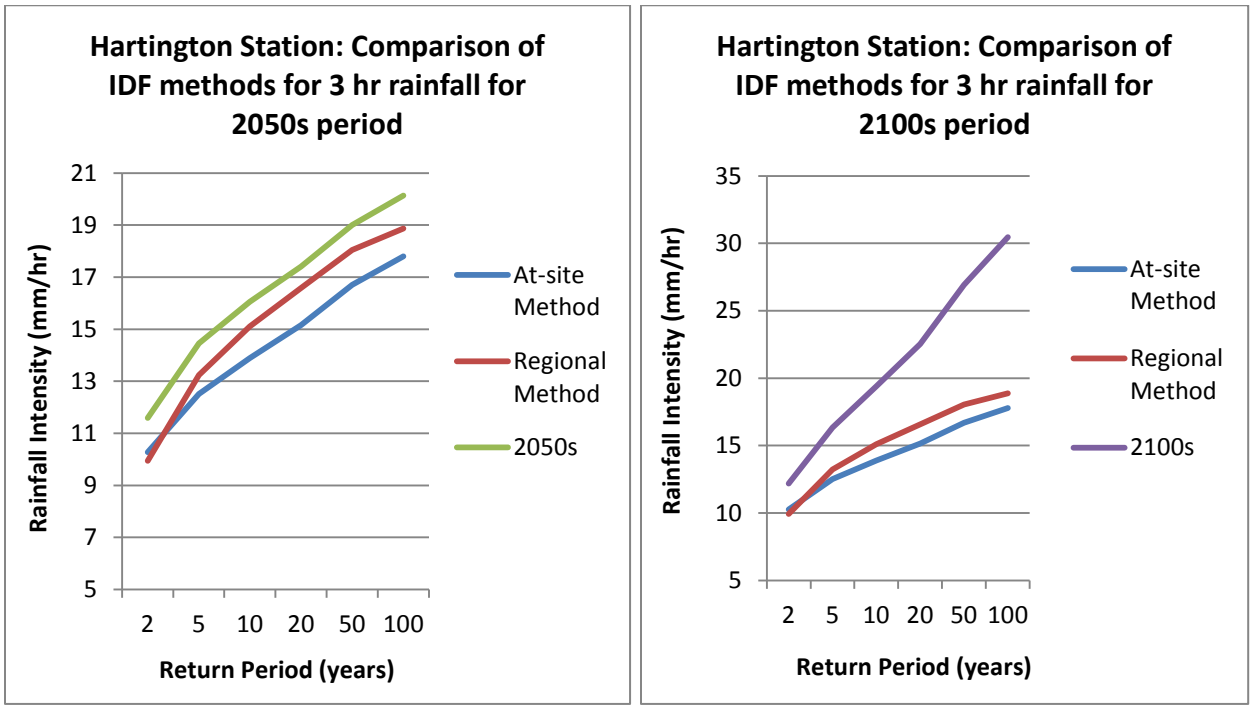

Figure 23: IDF curves obtained from the future IDF method, the regional frequency analysis method and the at-site method for Hartington station (cluster 6) for the 3 hour rainfall: *(a)* 2050s period and *(b)* 2100s time period.

(a) *(b)*

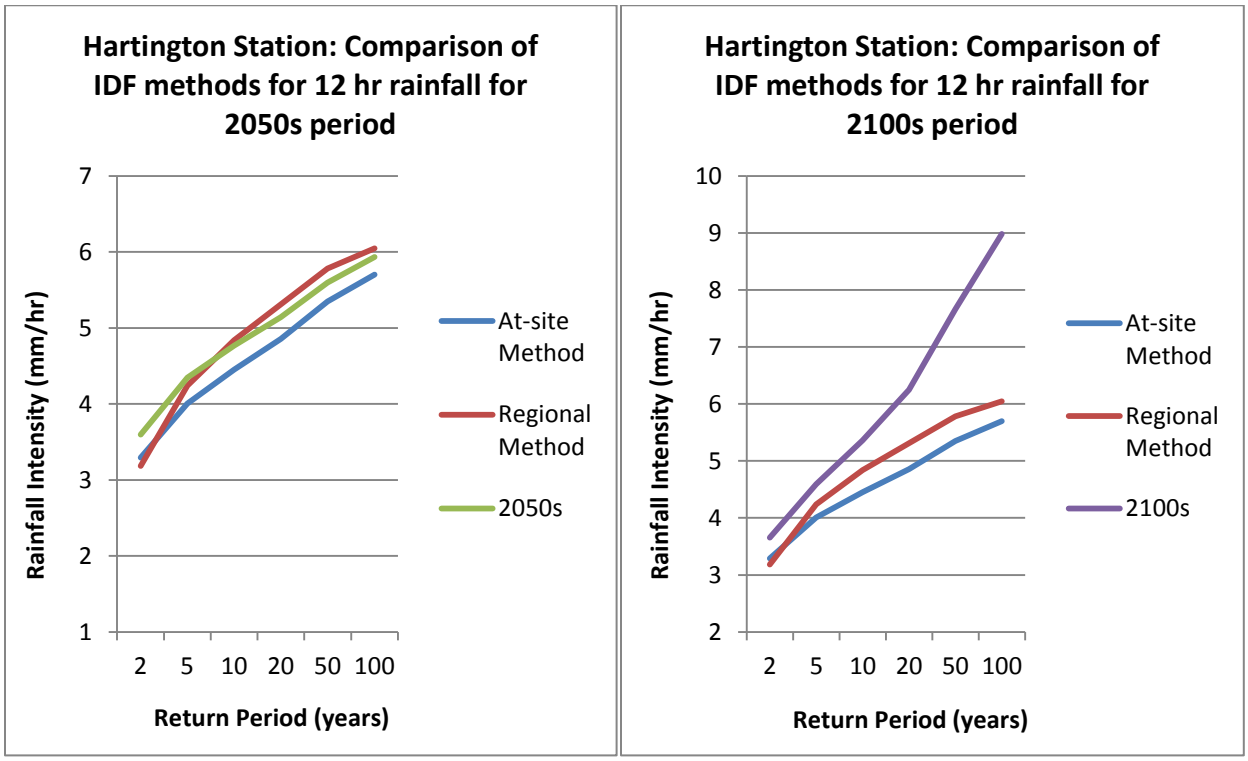

Figure 24: IDF curves obtained from the future IDF method, the regional frequency analysis method and the at-site method for Hartington station (cluster 6) for the 12 hour rainfall: *(a)* 2050s period and *(b)* 2100s time period.

The rainfall values obtained using the future IDF methods for Durham station and Hartington station showed that the 2050s time period had slightly larger rainfall values compared to the at-site IDF curve and the regional frequency analysis method IDF curve; the exception was for Hartington station 12 hour rainfall where the regional frequency analysis method had larger rainfall values for the 10, 20, 50 and 100 year return period compared to the 2050s period. The CanRCM4 and HadGEM2 climate models are based on the new IPCC emission scenarios which suggest that extreme increases in rainfall intensities will not be observed over a short timescale. As a result there were minor increases in rainfall values for the 2050s period. However, when comparing the 2100s time period to the at-site method and the regional frequency analysis method larger increases in rainfall values were observed for all return periods. Furthermore, the 2100s period had larger rainfall values for the 20, 50 and 100 year return periods when compared to the 2050s time period. Following the RCP4.5 and RCP8.5 emission scenarios it is expected that there will be large increases in rainfall values for the 2100s period (IPCC, 2014). (IPCC, 2014) infers that increases in extreme rainfall events will be realized over a large period of time due to the intensive greenhouse gas emissions that are projected to accumulate by the 2100s period. After developing IDF curves using the future IDF curve method it is expected that rainfall intensities are expected to significantly increase in southern Ontario for the 2100s period as similar results were observed for all stations in this region.

5.8 Variability of the Future IDF Curve Results

There are numerous climate models and emission scenarios that are available to create future IDF curves. Since infrastructure designs are planned to account for extreme rainfall events expected to occur in the future, it is important that climate models adequately represent projected

rainfall intensities for each respective region. The variability of results due to the diversity of the climate models and the associated emission scenarios was assessed as well.

For 12 hour rainfall duration for the Durham station, the climate model and emission scenario that produced the lowest intensity of rainfall for the 2100s period was the HadGEM2 model for the RCP4.5 emission scenario (Figure 24). The HadGEM2 model following the RCP4.5 scenario is an intermediate scenario where emission levels are supposed to level off, however, the rainfall intensity for this scenario are moderately larger compared to the at-site method rainfall intensities, therefore under one of the best case lowest emission scenarios, an increase in rainfall intensity is still expected for return periods greater than 10 years for the 2100s period. For the Durham station the climate model and emission scenario that produced the largest intensity of rainfall for the 2100s period was the CanRCM4 model for the RCP8.5 emission scenario. The rainfall intensities for this scenario are moderately larger compared to the at-site method rainfall intensities for the 2 – 10 year return periods however significant increases are observed for the 25 – 100 year return periods, therefore under one of the worst case emission scenarios a significant increase in rainfall intensity is expected for the 2100s period.

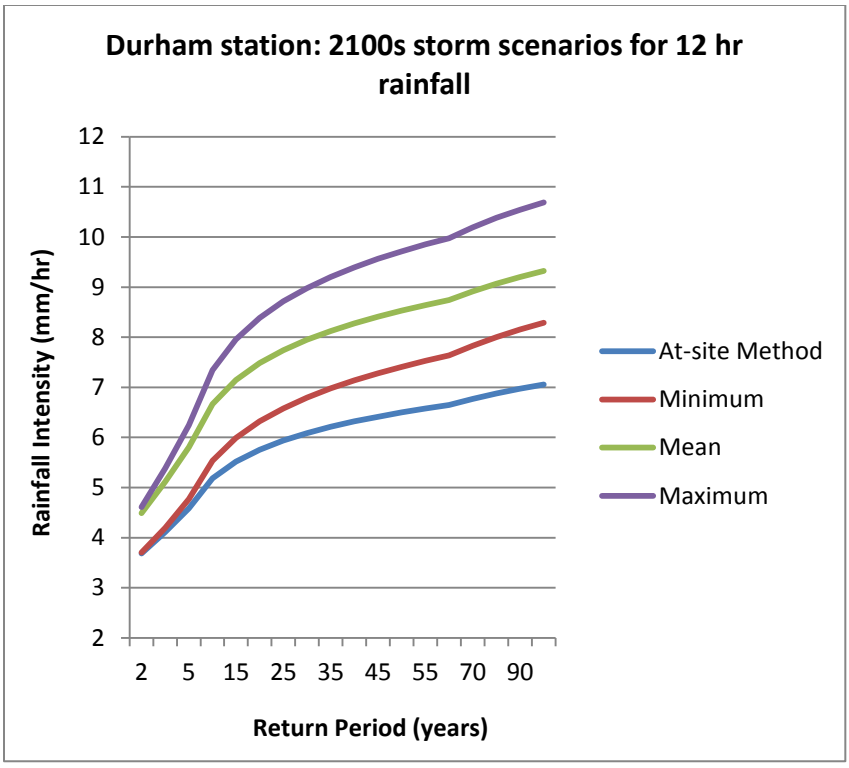

Figure 25: Comparison of IDF curves for 12 hour rainfall duration using the minimum, maximum and mean of the future IDF method results versus the at-site method results for Durham station. *Note: Minimum = HadGEM2 model following RCP4.5; Maximum = CanRCM4 model following RCP8.5; Mean = the average rainfall intensity of all climate models and emission scenarios used in this study.*

For 12 hour rainfall duration for the Hartington station, the climate model and emission scenario that produced the lowest intensity of rainfall for the 2100s period was the HadGEM2 model for the RCP4.5 emission scenario (Figure 26). The rainfall intensities for this scenario are smaller compared to the at-site method for short return periods (2 – 5 years), however the rainfall intensities for the 10 – 100 year return periods are larger compared to the at-site method rainfall intensities, therefore under one of the best case lowest emission scenarios an increase in rainfall intensity is still expected for all return periods for the 2100s period. For the Durham station the

climate model and emission scenario that produced the largest intensity of rainfall for the 2100s period was the CanRCM4 model for the RCP4.5 emission scenario. The rainfall intensities for this scenario are larger compared to the at-site method rainfall intensities for the 2 – 15 year return periods however significant increases are observed for the 20 – 100 year return periods, therefore following the RCP4.5 emission scenario a significant increase in rainfall intensity is expected for the 2100s period.

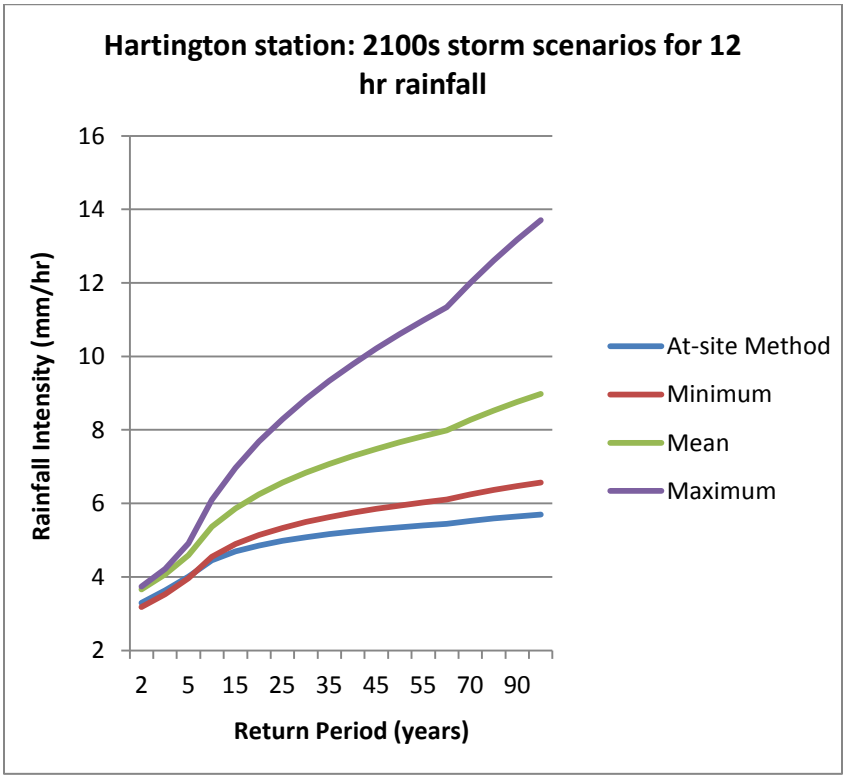

Figure 26: Comparison of IDF curves for 12 hour rainfall duration using the minimum, maximum and mean of the future IDF method results versus the at-site method results for Hartington station. *Note: Minimum = HadGEM2 model following RCP4.5; Maximum = CanRCM4 model following RCP4.5; Mean = the average rainfall intensity of all climate models and emission scenarios used in this study.*

Assessing the rainfall outputs for each climate model is of utmost importance to determine which climate models and emission scenarios should be utilized for research in the future. The climate models and emission scenarios used in this study showed that different scenarios can produce a wide range of rainfall intensities for both intermediate and extreme emission scenarios. In most cases the RCP8.5 emission scenario triggers the largest increase in rainfall intensities for the 2081 – 2099 period. The RCP4.5 emission scenario is associated with minimal increases in rainfall intensities for the 2081 – 2099 period, the only exception was for the 12 hour rainfall duration for Hartington station and in this case the RCP4.5 scenario was associated with the maximum increase in rainfall intensity. Pinpointing appropriate climate models and emission scenarios that will accurately represent future conditions will enable the derivation of IDF curves to be more accurate. Until then, using an ensemble of climate models to create IDF curves is the most effective method.

6. Discussion

Overall the three regionalization techniques used in this study produced different weather station clusters. PCA with k-means clustering and Ward's method created heterogeneous clusters. However Tabreg clustering method delineated statistically homogenous clusters that were contiguous. Tabreg clustering method incorporates a non-connectivity parameter in the cost function to ensure that delineated regions are compact and contiguous. Meanwhile PCA with k-means clustering and Ward's method do not incorporate a similar parameter in their objective function. Therefore using a regionalization technique that includes a factor which accounts for contiguity, such as Tabreg, is required to cluster stations into statistically homogeneous regions.

Furthermore, the at-site method IDF curves and the regional frequency analysis method IDF curves generated different rainfall values for each cluster. Using different probability distribution functions for the aforementioned methods resulted in the differences observed for the rainfall values. For different probability distribution functions the Z-score probability values are similar for short return periods (2, 5 and 10 year return periods). However for larger return periods (20, 50 and 100 year return periods) there are large differences in Z-score probability values. As a result the final IDF curve values for the regional frequency analysis method are larger than the rainfall values for the at-site method for all stations, especially for large return periods. There are multiple cases where clusters within the study area have different regional probability distribution functions compared to the at-site probability distribution function, as a result differences in rainfall values were observed in other clusters as well.

The rainfall values obtained using the future IDF curve methods showed that the 2050s time period had slightly larger rainfall values in comparison to the at-site method IDF curve and the regional frequency analysis method IDF curve. The IPCC emission scenarios describe that over a short period of time there will not be significant increases in rainfall intensities; subsequently there were insignificant increases in rainfall values for the 2050s period compared to the at-site method and regional frequency analysis method IDF curves. However, the 2100s period produced significantly larger rainfall values for the 20, 50 and 100 year return periods compared to the at-site method, regional frequency analysis method and the 2050s period. Under the RCP4.5 and RCP8.5 emission scenarios increases in rainfall intensities are expected over a large time scale due to the compilation of greenhouse gas emissions that will accumulate by the 2100s period. Consequently extreme rainfall events are expected for larger return periods during this time period. Therefore practitioners and organizations that are interested in updating

intensity-duration-frequency curves in a particular region of southern Ontario can recognize that accounting for future rainfall extremes for the 2100s period is essential for the design of hydraulic structures.

7. Conclusion

The IDF curves derived using the at-site method and the regional frequency analysis method for all stations produced different results. Comparing the at-site method using the GEV distribution for all sites with the regional frequency analysis method had previously not been completed in southern Ontario. Initial results showed that the regional frequency analysis method produced larger rainfall values compared to the at-site method for the 50 and 100 year return period. For most cases there were minor differences for rainfall intensities for 2 year, 5 year, 10 year and 20 year return periods.

Future IDF curves showed that for the 2050s time period there were minor increases in rainfall intensities when compared with the at-site method and the regional frequency analysis method whatever the region. For the 2100s time period there were larger increases in rainfall intensities compared to the at-site method and the regional frequency analysis method, especially for larger return periods (50 to 100 years). These results suggest that it is worthwhile for regions within southern Ontario to update their IDF curves using the future IDF curve technique, however further investigation to determine the most adequate climate models and emission scenarios is required.

This study also evaluated the ability of regionalization techniques such as Principal Component Analysis with k-means, Ward's method and Tabreg. The regionalization results indicate that only Tabreg was able to delineate contiguous homogeneous regions. The clusters

obtained using PCA with k-means and Ward's method were heterogeneous and therefore were not used for the regional IDF development in this study. Furthermore, most regionalization studies include latitude and longitude as inputs for clustering, and initially these two parameters were not included. However after including latitude and longitude as input parameters for PCA with k-means and Ward's method there was still little improvement in delineating contiguous homogeneous regions. Future research will attempt to include even more weather stations to see if homogeneous regions can be delineated using Tabreg with a larger number of stations.

Characterizing rainfall to determine future rainfall intensities in southern Ontario is of utmost importance to mitigate flooding impacts on society. The study results are consistent with previous studies and indicate that IDF curves should be updated in southern Ontario. Similar analysis approach should be applied to other study areas as well to ensure that IDF curves are created using adequate data and methods.

8. Recommendations

Based on the results found in this study the following recommendations can be made:

- Utilizing both global climate models or regional climate models are necessary to capture the future extreme rainfall trends which will enable accurate 100 year storm designs for new infrastructure. Using the Representative Concentration Pathways (RCP) emissions scenarios that represent intermediate to intensive greenhouse gas emissions is effective to eliminate any redundancies that might be caused by using lower emission scenarios. Therefore the strategies used in this study should be utilized when creating future IDF curves for additional weather stations in the study area.

- Further testing of probability distribution functions to ensure that we are characterizing extreme rainfall events properly is required using additional tests such as Mann-Kendall, Quantile-Quantile plots, Kolmogorov-Smirnov goodness of fit test and the Akaike Information Criterion (Coulibaly et al., 2015).
- Explore the possibility of using different parameter weights based on the importance of each input parameter for Tabreg. Also try using different input parameters for Tabreg such as extreme rainfall for 200 maximum values, for example.
- Since global climate models and regional climate models are continually evolving and being updated, using the latest version of the CRCM and HadGEM climate models for the next study is recommended.

9. References

Abolverdi, J., and Khalili, D., (2010). Development of Regional Rainfall Annual Maxima for Southwestern Iran by L-Moments. *Water Resources Management, 24*(11), 2501 – 2526.

Adamowski, J., Adamowski, K., Bougadis, J., (2010). Influence of Trend on Short Duration Design Storms. *Water Resources Management, 24*(3), 401 – 413.

Aguado, D., Montoya, T., Borras, L., Seco, A., and Ferrer, J., (2008). Using SOM and PCA for analysing and interpreting data from a P-removal SBR. *Engineering Applications of Artificial Intelligence, 21*(6), 919–930.

Bharath, R., and Srinivas, V.V., (2015). Regionalization of extreme rainfall in India. *International Journal of Climatology, 35*(6), 1142 – 1156.

Bernard, M. M., (1932). Formulas for rainfall intensities of long duration. *Transactions of the American Society of Civil Engineers, 96*(1), 592 – 606.

Bernard, E., Naveau, P., Vrac, M., Mestre, O., (2013). Clustering of maxima: Spatial dependencies among heavy rainfall in France. *Journal of Climate, 26*(20), 7929 – 7937.

Bozkaya, B., Erkut, E., and Laporte, G., (2003). A tabu search heuristic and adaptive memory procedure for political districting. *European Journal of Operational Research, 144*(1), 12 – 26.

Brunetti, M., Maugeri, M., Monti, F., and Nanni, T., (2004). Changes in daily precipitation frequency and distribution in Italy over the last 120 years. *Journal of Geophysical Research: Atmospheres, 109*(D5), 1 – 16.

Coulibaly, P., Burn, D.H., Switzman, H., Henderson, J., and Fausto, E., (2015). A Comparison of Future IDF Curves for Southern Ontario. Technical Report, Toronto Region Conservation Authority and Essex Region Conservation Authority, 1 – 100.

Coulibaly, P., and Shi, X., 2005. Identification of the Effect of Climate Change on Future Design Standards of Drainage Infrastructure in Ontario. Technical Report, Ministry of Transportation of Ontario.

City of Guelph, (2007). Frequency analysis of maximum rainfall and IDF design curve update (Technical Report). 1– 29.

Clavet-Gaumont, J., Sushama, L., Khaliq, M. N., Huziy, O., and Roy, R., (2013). Canadian RCM projected changes to high flows for Quebec watersheds using regional frequency analysis. *International Journal of Climatology, 33*(14), 2940 – 2955.

Conservation Halton, (2015). August 4th, 2014 Storm Event, Burlington. 1 – 35.

Davies, D. L., and Bouldin, D. W. (1979). A cluster separation measure. *IEEE transactions on pattern analysis and machine intelligence*, (2), 224-227.

Dominguez, F., Rivera, E., Lettenmaier, D.,P., and Castro, C. L., (2012). Changes in winter precipitation extremes for the western United States under a warmer climate as simulated by regional climate models. *Geophysical Research Letters, 39*(5), 1 – 7.

Environment and Climate Change Canada, (2014). Canada's Top 10 Weather Stories for 2013 – 2. Toronto's Torrent. *Climate and Historical Weather*, 3.

Feng, L., Zhou, T., Wu, B., Li, T., and Luo, J.J., (2011). Projection of future precipitation change over China with a high-resolution global atmospheric model. *Advances in Atmospheric Sciences, 28*(2), 464 – 476.

Fragoso, M., and Tildes Gomes, P., (2008). Classification of daily abundant rainfall patterns an associated large-scale atmospheric circulation types in southern Portugal. *International Journal of Climatology, 28*(4), 537 – 544.

Hennessy, K. J., Gregory, J. M., and Mitchell, J. F. B., (1997). Changes in daily precipitation under enhanced greenhouse conditions. *Climate Dynamics, 13*, 667 – 680.

Hershfield, D.M., (1961). Rainfall Frequency Atlas of the United States for Durations from 30 minutes to 24 hours and Return Periods from 1 to 100 Years. *U.S. Weather Bureau, Technical Paper 40*.

Hosking, J.R.M., and Wallis, J.R., (1997). Regional Frequency Analysis An Approach Based on L-moments. Cambridge University Press.

Huff, F.A., and Angel, J.R., (1989). Frequency Distribution and Hydraulic Climatic Characteristics of Heavy Rainstorms in Illinois, Bulletin 70, Illinois State Water Survey, Champaign, Illinois.

Huff, F.A., and Angel, J.R., (1992). Rainfall Frequency Atlas of the Midwest, Bulletin 71, Midwestern Climate Center and Illinois State Water Service, 1992, 5 – 6.

Hydrological Atlas of Canada, (1978). Fisheries and Environment Canada.

Intergovernmental Panel on Climate Change, (2014). Climate Change 2014: Synthesis Report. *Contribution of Working Groups I, II and III to the Fifth Assessment Report of the*

Intergovernmental Panel on Climate Change [Core Writing Team, R.K. Pachauri and L.A. Meyer (eds.)]. IPCC, Geneva, Switzerland, 151.

Jingyi, Z., and Hall, M.J., (2004). Regional flood frequency analysis for the Gan-Ming River basin in China. *Journal of Hydrology, 296*, 98 – 117.

Kahya, E., Demirel, M.C., Bég, O.A., (2008). Hydrologic homogeneous regions using monthly streamflow in Turkey. *Earth Sciences Research Journal, 12*(2), 181 – 193.

Kansakar, S. R., Hannah, D. M., Gerrard, J., Rees, G., (2004). Spatial pattern in the precipitation regime of Nepal. *International Journal of Climatology, 24*(13), 1645 – 1659.

Kyselý, J., Picek, J., and Huth, R., (2007). Formation of homogeneous regions for regional frequency analysis of extreme precipitation events in the Czech Republic. *Studia Geophysica et Geodaetica, 51*(2), 327 – 344.

Lemmen, D.S., Warren, F.J., Lacroix, J., and Bush, E., editors (2008). From Impacts to Adaptation: Canada in a Changing Climate 2007. Government of Canada, Ottawa, Ontario.

Lim, Y.H., and Voeller, D.L., (2009). Regional flood estimations in Red River using L-moment based index-flood and Bulletin 17B procedures. *Journal of Hydrologic Engineering, 14*(9), 1002 – 1016.

Lin, G.F., and Chen, L.H., (2006). Identification of homogeneous regions for regional frequency analysis using the self-organizing map. *Journal of Hydrology, 324*(1), 1 – 9.

Mailhot, A., Duchesne, S., Caya, D., and Talbot, G., (2007). Assessment of future change in intensity-duration-frequency (IDF) curves for Southern Quebec using the Canadian Regional Climate Model (CRCM). *Journal of Hydrology, 347*(1), 197 – 210.

Mailhot, A., Beauregard, I., Talbot, G., Caya, D., and Biner, S., (2012). Future changes in intense precipitation over Canada assessed from multi-model NARCCAP ensemble simulations. *International Journal of Climatology, 32*(8), 1151 – 1163.

Malekinezhad, H., and Zare-Garizi, A., (2014). Regional frequency analysis of daily rainfall extremes using L-moments approach. *Atmósfera, 27*(4), 411 – 427.

Mallants, D., and Feyen, J., (1990). Defining homogeneous precipitation regions by means of principal componenet analysis. *Journal of Applied Meterology, 29,* 892 – 901.

Maraun, D., Osborn, T.J., and Gilleet, N.P., (2008). United Kingdom daily precipitation intensity: improved early data, error estimates and an update from 2000 to 2006. *International Journal of Climatology, 28*(6), 833 – 842.

Marengo, J.A., Ambrizzi, T., da Rocha, R.P., Alves, L.M., Cuadra, S.V., Valverde, M.C., Torres, R.R., Santos, D.C., Ferraz, S.E.T, (2010). Future change of climate in South America in the late twenty-first century: Intercomparison of scenarios from three regional climate models. *Climate Dynamics, 35*(6), 1089 – 1113.

Mladjic, B., Sushama, L., Khaliq, M.N., Laprise, R., Caya, D., and Roy, R., (2011). Canadian RCM projected changes to extreme precipitation characteristics over Canada. *Journal of Climate, 24*(10), 2565 – 2584.

Modarres, R., and Sarhadi, A., (2011). Statistically-based regionalization of rainfall climates of Iran. *Global and Planetary Change, 75*(1), 67 – 67.

Muñoz-Diaz, D., and Rodrigo, F.S., (2004). Spatio-temporal patterns of seasonal rainfall in Spain (1912 – 2000) using cluster and principal component analysis : comparison. *Annales Geophysicae, 22*, 1435 – 1448.

Nam, W., Shin, H., Jung, Y., Joo, K., and Heo, J.H., (2015). Delineation of the climatic rainfall regions of South Korea based on a multivariate analysis and regional rainfall frequency analyses. *International Journal of Climatology, 35*(5), 777 – 793.

Ngongondo, C.S., Xu, C.Y., Tallaksen, L.M., Alemaw, B., and Chirwa, T., (2011). Regional frequency analysis of rainfall extremes in Southern Malawi using the index rainfall and L-moments approaches. *Stochastic Environmental Research and Risk Assessment, 25*(7), 939 – 955.

Noto, L., and La Loggia, G., (2009). Use of L-moments approach for regional flood frequency analysis in Sicily, Italy. *Water Resources Management, 23*(11), 2207 – 2229.

Olsson, J., Berggren, K., Olofsson, M., and Viklander, M., (2009). Applying climate model precipitation scenarios for urban hydrological assessment: A case study in Kalmar City, Sweden. *Atmospheric Research, 92*(3), 364 – 375.

Paixao, E., Auld, H., Mirza, M.M.Q., Klaassen, J., and Shephard, M.W., (2011). Regionalization of heavy rainfall to improve climatic design values for infrastructure: case study in Southern Ontario, Canada. *Hydrological Sciences Journal, 56*(7), 1067 – 1089.

Parida, B.P., and Moalafhi, D.B., (2008). Regional rainfall frequency analysis for Botswana using L-Moments and radial basis function network. *Physics and Chemistry of the Earth, 33*, 614 – 620.

Razavi, T., and Coulibaly, P., (2013). Classification of Ontario watersheds based on physical attributes and streamflow series. *Journal of Hydrology, 493*, 81 – 94.

Saf, B., (2009). Regional Flood Frequency Analysis Using L Moments for the Buyuk and Kucuk Menderes River Basins of Turkey. *Journal of Hydrologic Engineering, 14*(8), 783 – 794.

Schaefer, M.G., Barker, B.L., Taylor, G.H., and Wallis, J.D., (2006). Regional precipitation frequency analysis and spatial mapping of precipitation for 24-hour and 2-hour durations in eastern Washington. *Washington State Department of Transportation*, 1 – 40.

Shephard, M.W., (2011). Updating IDF Climate Design Values for the Atlantic Provinces. Ministry of Environment, Labour and Justice, Government of Prince Edward Island.

Smithers, J.C., and Schulze R.E., (2001). A methodology for the estimation of short duration design storms in South Africa using a regional approach based on L-moments. *Journal of Hydrology, 241*(1), 42 – 52.

Stathis, D., and Myronidis, D., (2009). Principal Component Analysis of Precipitation in Thessaly Region (Central Greece). *Global NEST Journal, 11*(4), 467 – 476.

SUDPLAN 2012: Sustainable Urban Development Planner for Climate Change Adaptation. Project 247708, Final Report Available online at:

http://sudplan.eu/polopoly_fs/1.30418!/SUDPLAN_final.pdf

Trefry, C.M., Watkins Jr., D.W., and Johnson, D., (2005). Regional Rainfall Frequency Analysis for the State of Michigan. *Journal of Hydrologic Engineering, 10*(6), 437 – 449.

Unal, Y., Kindap, T., and Karaca, M., (2003). Redefining the climate zones of Turkey using cluster analysis. *International Journal of Climatology, 23*(9), 1045 – 1055.

Urrutia, R., and Vuille, M., (2009). Climate change projections for the tropical Andes using a regional climate model: Temperature and precipitation simulations for the end of the 21st century. *Journal of Geophysical Research Atmospheres, 114*(2), 1 – 15.

Willems, P., Arnbjerg-Nielsen, K., Olsson, J., and Nguyen, V.T.V., (2012). Climate change impact assessment on urban rainfall extremes and urban drainage: methods and shortcomings. *Atmospheric Research, 103*, 106 – 118.

Xuejie, G., Zongci, Z., Yihui, D., Ronghui, H., and Giorgi, F., (2001). Climate change due to greenhouse effects in China as simulated by a regional climate model. *Advances in Atmospheric Sciences, 18*(6), 1224 – 1230.

Yiannakoulias, N., Rosychuk, R.J., and Hodgson, J., (2007). Adaptations for finding irregularly shaped disease clusters. *International Journal of Health Geographics, 6*.

Yiannakoulias, N., and Bland, W., (2016). Tabreg: Software for Regionalization Problems. Health Geomatics Lab, School of Geography and Earth Sciences, McMaster University.

Appendix A

Station Name	Latitude	Longitude	Elevation (meters)
Belleville	44.15	-77.39	76.2
Bloomfield	43.98	-77.22	91.4
Bowmanville MOSTERT	43.92	-78.67	99.1
Brantford MOE	43.13	-80.23	196.0
Burketon Mclaughlin	44.03	-78.80	312.4
Chatham	42.39	-82.22	180.0
Chatsworth	44.40	-80.91	305.0
Cressy	44.10	-76.85	83.8
Durham	44.18	-80.82	384.0
Fergus Shand Dam	43.73	-80.33	417.6
Foldens	43.02	-80.78	328.0
Fort Erie	42.88	-78.97	179.8
Frechmans Bay	43.82	-79.08	76.2
Georgetown WWTP	43.64	-79.88	221.0
Glen Allan	43.68	-80.71	400.0
Glen Haffy Mono Mills	43.93	-79.95	434.3
Hagersville	42.97	-80.07	221.0
Hamilton Airport	43.17	-79.93	237.7
Hartington IHD	44.43	-76.69	160.0
Kingston Pumping Station	44.24	-76.48	76.5
Kingsville MOE	42.04	-82.67	200.0
London International Airport	43.03	-81.15	278.0
Millgrove	43.32	-79.97	255.1
New Glasgow	42.51	-81.64	198.1
Oakville Southeast WPCP	43.48	-79.63	86.9
Orangville MOE	43.92	-80.09	411.5
Oshawa WPCP	43.87	-78.83	83.8

Owen Sound MOE	44.58	-80.93	178.9
Petrolia Town	42.88	-82.17	201.2
Port Colborne	42.88	-79.25	175.3
Proton Station	44.17	-80.52	480.1
Richmond Hill	43.88	-79.45	240.0
Ridgeville	43.04	-79.33	236.2
Sarnia Airport	42.99	-82.30	180.6
St. Catharines Power Glen	43.12	-79.25	121.9
Stratford WWTP	43.37	-81.00	345.0
Thornbury Slama	44.57	-80.49	213.4
Thornhill Grandview	43.80	-79.42	199.3
Tillsonburg WWTP	42.86	-80.72	213.4
Toronto Island Airport	43.63	-79.40	76.5
Toronto Pearson Airport	43.68	-79.63	173.4
Trenton Airport	44.12	-77.53	86.3
Vineland Rittenhouse	43.17	-79.42	94.5
Waterloo Wellington	43.45	-80.38	317.0
Welland	42.99	-79.26	175.3
Wiarton Airport	44.75	-81.11	222.2
Windsor Airport	42.28	-82.96	189.6
Woodstock	43.14	-80.77	281.9

Table A1: Geographic characteristics of each weather station.

Appendix B

	Environment Canada Flagged Data						
Station Name	T	C	A	E	F	"blank" cells	M
Belleville	1750	2	2	92	0	0	0
Bloomfield	493	50	43	158	5	31	8
Bowmanville MOSTERT	668	2	2	28	0	62	1
Brantford MOE	579	17	8	98	6	92	24
Burketon Mclaughlin	494	7	2	86	6	59	18
Chatham	382	24	26	32	0	62	0
Chatsworth	901	11	10	38	1	0	0
Cressy	814	7	7	29	0	424	8
Durham	1455	99	86	153	1	152	43
Fergus Shand Dam	751	1	1	15	0	91	0
Foldens	1241	6	4	60	0	0	0
Fort Erie	1100	19	20	75	0	155	41
Frechmans Bay	1191	17	16	5	0	120	0
Georgetown WWTP	867	17	16	36	2	243	9
Glen Allan	957	1	0	13	1	62	0
Glen Haffy Mono Mills	458	31	19	137	9	242	12
Hagersville	1039	8	8	28	0	0	0
Hamilton Airport	1686	0	0	0	0	60	0
Hartington IHD	944	10	8	33	1	31	1
Kingston Pumping Station	1186	1	1	4	0	31	1
Kingsville MOE	1210	29	30	65	1	31	6
London International Airport	1751	0	0	3	0	20	7
Millgrove	491	18	17	152	4	153	96
New Glasgow	123	13	12	37	0	61	1
Oakville Southeast WPCP	418	33	18	183	10	304	50
Orangville MOE	647	10	7	73	3	62	10
Oshawa WPCP	656	2	2	32	0	62	0
Owen Sound MOE	656	10	5	95	4	30	1

Petrolia Town	354	12	11	41	0	31	31
Port Colborne	534	8	7	35	2	181	1
Proton Station	644	1	1	16	0	0	0
Richmond Hill	1314	0	0	4	0	61	0
Ridgeville	762	41	29	154	7	124	23
Sarnia Airport	1397	0	0	4	0	0	6
St. Catharines Power Glen	735	65	45	221	11	241	86
Stratford WWTP	1372	1	1	14	0	31	0
Thornbury Slama	712	12	11	48	0	0	0
Thornhill Grandview	911	5	4	24	1	31	0
Tillsonburg WWTP	772	35	27	83	4	28	12
Toronto Island Airport	1439	0	0	12	0	22	163
Toronto Pearson Airport	2319	0	0	0	0	60	0
Trenton Airport	1973	0	0	0	0	55	0
Vineland Rittenhouse	666	6	5	16	0	0	0
Waterloo Wellington Airport	1388	0	0	0	0	60	0
Welland	945	2	2	30	0	242	8
Wiarton Airport	1319	0	0	0	0	178	3
Windsor Airport	1872	0	0	0	0	67	0
Woodstock	1049	8	6	84	2	59	11

Table B1: List of flagged data found for each weather station. *Note:* The definition for each flagged value is provided in the table below

Flag	Definition	Replaced Value
A	Accumulated amount; previous value was C.	0 mm
C	Precipitation occurred, amount uncertain.	0 mm
E	Estimated.	Flag was removed; daily precipitation value was provided by EC.
F	Accumulated and estimated.	Flag was removed; daily precipitation value was provided by EC.
M	Missing.	The linear regression value from nearest neighbouring station was used.
T	Trace.	0.2 mm
“blank” cells	Missing.	The linear regression value from nearest neighbouring station was used.

Table B2: Definition of each flag data that was found in the daily precipitation data. The method that was used to replace each of the flag data is indicated in the table. *Note:* EC is an acronym for Environment Canada

Appendix C

Climate Model	Spatial Resolution	Scenario	Temporal Resolution	Simulation Period
CanRCM4-CanEMS2	40 km	Historical	1 hour	1970 – 2000
		RCP 4.5	1 hour	2006 – 2100
		RCP 8.5	1 hour	2006 – 2100
HadGEM2-ES	1.25 × 1.875 degrees (approximately 120 km x 139 km)	Historical	3 hour	1970 – 2000
		RCP 4.5	3 hour	2026 – 2045; 2081 – 2099
		RCP 8.5	3 hour	2026 – 2045; 2081 – 2099

Table C1: Data and resolution of the CanRCM4-CanEMS2 and HadGEM2-ES climate models used.

Appendix D

Site 15 Glen Allan: At-site Method IDF Curve Results						
Return Period	1 hour	2 hours	3 hours	6 hours	12 hours	24 hours
2 years	24.5	15.3	11.6	6.6	3.7	2.3
5 years	31.9	19.9	15.1	8.6	4.8	3.0
10 years	37.0	23.0	17.6	10.0	5.6	3.4
20 years	42.1	26.2	20.0	11.4	6.4	3.9
50 years	49.0	30.5	23.2	13.3	7.4	4.5
100 years	54.4	33.9	25.8	14.7	8.3	5.0

Table D1: IDF values for Glen Allan station using the at-site method.

Site 15 Glen Allan: RFA Method IDF Curve Results						
Return Period	1 hour	2 hours	3 hours	6 hours	12 hours	24 hours
2 years	24.3	15.1	11.5	6.6	3.7	2.2
5 years	31.6	19.7	15.0	8.5	4.8	2.9
10 years	37.2	23.2	17.7	10.1	5.7	3.4
20 years	43.5	27.1	20.6	11.8	6.6	4.0
50 years	53.3	33.1	25.2	14.4	8.1	4.9
100 years	62.1	38.6	29.4	16.8	9.4	5.8

Table D2: IDF values for Glen Allan station using the regional frequency analysis method.

Site 39 Tillsonburg: At-site Method IDF Curve Results						
Return Period	1 hour	2 hours	3 hours	6 hours	12 hours	24 hours
2 years	24.8	15.5	11.8	6.7	3.8	2.3
5 years	31.0	19.3	14.7	8.4	4.7	2.9
10 years	35.2	21.9	16.7	9.5	5.3	3.3
20 years	39.4	24.5	18.7	10.7	6.0	3.6
50 years	45.1	28.0	21.4	12.2	6.8	4.2
100 years	49.4	30.8	23.4	13.4	7.5	4.6

Table D3: IDF values for Tillsonburg station using the at-site method.

Site 39 Tillsonburg: RFA Method IDF Curve Results						
Return Period	1 hour	2 hours	3 hours	6 hours	12 hours	24 hours
2 years	24.2	15.1	11.5	6.6	3.7	2.2
5 years	31.6	19.6	15.0	8.5	4.8	2.9
10 years	37.2	23.1	17.6	10.1	5.6	3.4
20 years	43.4	27.0	20.6	11.7	6.6	4.0
50 years	53.2	33.1	25.2	14.4	8.1	4.9
100 years	62.0	38.6	29.4	16.8	9.4	5.7

Table D4: IDF values for Tillsonburg station using the regional frequency analysis method.

Site 43 Vineland Rittenhouse: At-site Method IDF Curve Results						
Return Period	1 hour	2 hours	3 hours	6 hours	12 hours	24 hours
2 years	23.0	14.3	10.9	6.2	3.5	2.1
5 years	28.5	17.7	13.5	7.7	4.3	2.6
10 years	31.7	19.8	15.1	8.6	4.8	2.9
20 years	34.7	21.6	16.5	9.4	5.3	3.2
50 years	38.3	23.8	18.1	10.3	5.8	3.5
100 years	40.7	25.3	19.3	11.0	6.2	3.8

Table D5: IDF values for Vineland Rittenhouse station using the at-site method.

Site 43 Vineland Rittenhouse: RFA Method IDF Curve Results						
Return Period	1 hour	2 hours	3 hours	6 hours	12 hours	24 hours
2 years	22.2	13.8	10.5	6.0	3.4	2.1
5 years	28.7	17.9	13.6	7.8	4.4	2.7
10 years	33.2	20.7	15.8	9.0	5.0	3.1
20 years	37.9	23.6	18.0	10.2	5.8	3.5
50 years	44.2	27.5	21.0	12.0	6.7	4.1
100 years	49.2	30.6	23.3	13.3	7.5	4.6

Table D6: IDF values for Vineland Rittenhouse station using the regional frequency analysis method.

Site 17 Hagersville: At-site Method IDF Curve Results						
Return Period	1 hour	2 hours	3 hours	6 hours	12 hours	24 hours
2 years	25.2	15.7	12.0	6.8	3.8	2.3
5 years	32.2	20.1	15.3	8.7	4.9	3.0
10 years	37.0	23.0	17.6	10.0	5.6	3.4
20 years	41.8	26.0	19.8	11.3	6.3	3.9
50 years	48.2	30.0	22.8	13.0	7.3	4.5
100 years	53.1	33.0	25.2	14.4	8.1	4.9

Table D7: IDF values for Hagersville station using the at-site method.

Site 17 Hagersville: RFA Method IDF Curve Results						
Return Period	1 hour	2 hours	3 hours	6 hours	12 hours	24 hours
2 years	24.7	15.4	11.7	6.7	3.8	2.3
5 years	32.2	20.0	15.3	8.7	4.9	3.0
10 years	37.7	23.5	17.9	10.2	5.7	3.5
20 years	43.5	27.1	20.6	11.8	6.6	4.0
50 years	51.8	32.2	24.5	14.0	7.9	4.8
100 years	58.6	36.5	27.8	15.8	8.9	5.4

Table D8: IDF values for Hagersville station using the regional frequency analysis method.

Appendix E

Durham 3 hour rainfall IDF Curve Comparison				
Return Period	At-site Method	RFA Method	2050s Period	2100s period
2 years	11.5	11.5	12.7	14.8
5 years	14.3	14.6	16.3	18.5
10 years	16.2	16.6	18.3	20.8
20 years	18.0	18.5	20.1	22.9
50 years	20.3	20.9	22.2	25.6
100 years	22.0	22.7	23.5	27.7

Table E1: IDF values for Durham station (3 hour rainfall) using the at-site method, regional frequency analysis method and future IDF curve development method.

Durham 12 hour rainfall IDF Curve Comparison				
Return Period	At-site Method	RFA Method	2050s Period	2100s period
2 years	3.7	3.7	4.0	4.5
5 years	4.6	4.7	5.1	5.8
10 years	5.2	5.3	5.6	6.7
20 years	5.8	5.9	6.1	7.5
50 years	6.5	6.7	6.8	8.5
100 years	7.1	7.3	7.3	9.3

Table E2: IDF values for Durham station (12 hour rainfall) using the at-site method, regional frequency analysis method and future IDF curve development method.

Hartington 3 hour rainfall IDF Curve Comparison				
Return Period	At-site Method	RFA Method	2050s Period	2100s period
2 years	10.3	9.9	11.6	12.2
5 years	12.5	13.2	14.5	16.4
10 years	13.9	15.1	16.0	19.4
20 years	15.2	16.6	17.4	22.5
50 years	16.7	18.0	19.0	26.9
100 years	17.8	18.9	20.1	30.5

Table E3: IDF values for Hartington station (3 hour rainfall) using the at-site method, regional frequency analysis method and future IDF curve development method.

Hartington 12 hour rainfall IDF Curve Comparison				
Return Period	At-site Method	RFA Method	2050s Period	2100s period
2 years	3.3	3.2	3.6	3.7
5 years	4.0	4.2	4.3	4.6
10 years	4.5	4.8	4.8	5.4
20 years	4.9	5.3	5.1	6.2
50 years	5.4	5.8	5.6	7.7
100 years	5.7	6.0	5.9	9.0

Table E4: IDF values for Hartington station (12 hour rainfall) using the at-site method, regional frequency analysis method and future IDF curve development method.